World Academy of Science, Engineering and Technology
International Journal of Mechanical and Mechatronics Engineering
Vol:5, No:3, 2011

Flat Miniature Heat Pipes for Electronics Cooling: State of the Art, Experimental and Theoretical Analysis

M.C. Zaghdoudi, S. Maalej, J. Mansouri, and M.B.H. Sassi

***Abstract*—**An experimental study is realized in order to verify the Mini Heat Pipe (MHP) concept for cooling high power dissipation electronic components and determines the potential advantages of constructing mini channels as an integrated part of a flat heat pipe. A Flat Mini Heat Pipe (FMHP) prototype including a capillary structure composed of parallel rectangular microchannels is manufactured and a filling apparatus is developed in order to charge the FMHP. The heat transfer improvement obtained by comparing the heat pipe thermal resistance to the heat conduction thermal resistance of a copper plate having the same dimensions as the tested FMHP is demonstrated for different heat input flux rates. Moreover, the heat transfer in the evaporator and condenser sections are analyzed, and heat transfer laws are proposed. In the theoretical part of this work, a detailed mathematical model of a FMHP with axial microchannels is developed in which the fluid flow is considered along with the heat and mass transfer processes during evaporation and condensation. The model is based on the equations for the mass, momentum and energy conservation, which are written for the evaporator, adiabatic, and condenser zones. The model, which permits to simulate several shapes of microchannels, can predict the maximum heat transfer capacity of FMHP, the optimal fluid mass, and the flow and thermal parameters along the FMHP. The comparison between experimental and model results shows the good ability of the numerical model to predict the axial temperature distribution along the FMHP.

***Keywords*—**Electronics Cooling, Micro Heat Pipe, Mini Heat Pipe, Mini Heat Spreader, Capillary grooves.

NOMENCLATURE

A	Constant in Eq. (16), Section, m²
B	Bias contributor to the uncertainty
C_p	Specific heat, J/kg.K
d	Side of the square microchannel, m
D_g	Groove height, m
D_h	Hydraulic diameter, m
f	Friction factor
g	Gravity acceleration, m/s²
h	Heat transfer coefficient, W/m².K
I	Current, A
Ja*	Modified Jacob number
k	Poiseuille number
l	Width, m
L	FMHP overall length, m
La	Laplace constant, m
l_c	Condenser width, m
L_c	Condenser length, m
l_e	Evaporator width, m
L_e	Evaporator length, m
L_{eff}	FMHP effective length, m
$\dot{m}$	Mass flow rate, kg/s
m_1	Constant in equation (16)
m_2	Constant in equation (16)
m_3	Constant in equation (16)
N_g	Number of grooves
Nu	Nüsselt number
P	Equipment precision contributor to uncertainty, Pressure, N/m²
Pr	Prandtl number
q	Heat flux, W/m²
Q	Heat transfer rate, W
Q_a	Axial heat flux rate, W
r_c	Radius of curvature, m
Re	Reynolds number
R_{th}	Thermal resistance, K/W
S_g	Groove spacing, m
S	Heat transfer area, m²
S_g	Groove spacing, m
t	Thickness, m
T	Temperature, °C
T_c	Wall condenser temperature, °C
T_{ev}	Wall evaporator temperature, °C
T_f	Film temperature, °C
T_{sf}	Heat sink temperature, °C
T_w	Wall temperature, °C
U	Uncertainty
V	Voltage, V
V_e	Velocity, m/s
w	Axial velocity, m/s
W	FMHP width, m
W_g	Groove width, m
z	Coordinate, m

M. C. Zaghdoudi is with the University of Carthage, National Institute of Applied Sciences and Technology (INSAT), Unit of Research Materials, Measurements, and Applications (MMA), Centre Urbain Nord BP N° 676 – 1080 Tunis, Tunisia (phone: (216) 71 704 309; fax: (216) 71 704 329 (e-mail: chaker.zaghdoudi@insat.rnu.tn).

S. Maalej is with the University of Carthage, National Institute of Applied Sciences and Technology (INSAT), Unit of Research Materials, Measurements, and Applications (MMA), Centre Urbain Nord BP N° 676 – 1080 Tunis, Tunisia (phone: (216) 71 704 309; fax: (216) 71 704 329 (e-mail: samah.maalej@insat.rnu.tn).

J. Mansouri is with the University of Carthage, National Institute of Applied Sciences and Technology (INSAT), Unit of Research Materials, Measurements, and Applications (MMA), Centre Urbain Nord BP N° 676 – 1080 Tunis, Tunisia (phone: (216) 71 704 309; fax: (216) 71 704 329 (e-mail: jadmansouri@yahoo.fr).

M.B.H. Sassi is with University of Carthage, National Institute of Applied Sciences and Technology (INSAT), Unit of Research Materials, Measurements, and Applications (MMA), Centre Urbain Nord BP N° 676 – 1080 Tunis, Tunisia (phone: (216) 71 704 309; fax: (216) 71 704 329 (e-mail: jadmansouri@yahoo.fr).

Greek Symbols

α	Contact angle, °
β	Tilt angle, °
ΔT	Temperature difference = $T_{ev} - T_c$, K
Δh_v	Latent heat of vaporization, J/kg
ΔP	Pressure drop, N/m²
λ	Thermal conductivity, W/m.K
μ	Dynamic viscosity, kg/m.s
θ	Angle defined by Eq. (29), °
ρ	Density, kg/m^3
σ	Surface tension, N/m
τ	Shear stress, N/m²

Subscripts and superscripts

a	Adiabatic
b	Blocked
c	Condenser, Curvature
d	Dry
Cu	Copper
ev	Evaporator
eff	Effective
eq	Equivalent
exp	Experimental
f	Film
il	Interfacial (liquid side)
iv	Interfacial (vapor side)
l	Liquid
lw	Liquid-Wall
max	Maximum
min	Minimum
sat	Saturation
sf	Heat sink
t	Total
v	Vapor
vw	Vapor-Wall
w	Wall

I. INTRODUCTION

Thermal management of electronic components must solve problems connected with the limitations on the maximum chip temperature and the requirements of the level of temperature uniformity. To cool electronic components, one can use air and liquid coolers as well as coolers constructed on the principle of the phase change heat transfer in closed space, i.e. immersion, thermosyphon and heat pipe coolers. Each of these methods has its merits and draw-backs, because in the choice of appropriate cooling one must take into consideration not only the thermal parameters of the cooler, but also design and stability of the system, durability, technology, price, application, etc.

Heat pipes represent promising solutions for electronic equipment cooling [1]. Heat pipes are sealed systems whose transfer capacity depends mainly on the fluid and the capillary structure. Several capillary structures are developed in order to meet specific thermal needs. They are constituted either by an integrated structure of microchannels or microgrooves machined in the internal wall of the heat spreader, or by porous structures made of wire screens or sintered powders. According to specific conditions, composed capillary structures can be integrated into heat pipes.

Heat pipes are not in general a low cost solution to the cooling problem, but it is most effective and has great potential as power levels and volume requirements increase. For these reasons heat pipes have been applied up to now mainly in application with special working conditions and requirements such as in space thermal control, in aircraft devices, in traction drives, in audio amplifiers, in cooling of closed cabinets in harsh environmental conditions, etc.

It is anticipated that future applications of the heat dissipation device will have to work along with small efficient devices. The electronic heat dissipation components are required to have smaller size and to be more efficient. The Flat Miniature Heat Pipes (FMHPs) are one of such devices to meet the requirement, which have developed in different ways and layouts, according to its materials, capillary structure design and manufacturing technology.

Despite the advances in FMHPs designs, most of them, especially those including grooves, reveal only the functionality during horizontal operation, with few FMHPs successfully demonstrating adverse-gravity or acceleration functionality. These studies show that the manufacture of FMHPs that maintain the same performance for all operational orientations is a problem yet to be overcome.

The operation of the FMHPs is governed by the wick structure. The narrower the wick structure, the higher is the capillary pumping. Although a sintered wick processes larger capillary forces, however it demonstrates large contact thermal resistance and large liquid flow resistance, which influence its practical application. An axially grooved FMHP has a thinner wall, lighter weight, and smaller thermal resistance. Since the key point of such FMHPs operation is the grooves, their fabrication techniques and processes are of great importance. This feature will enhance the geometry dimension of the grooves and the heat transfer capacity further.

The fabrication of narrow grooves in size is a challenging task for conventional machining techniques. Accordingly, a number of different techniques including high speed dicing, electro-discharge machining, and laser micromachining have been applied to the fabrication of metallic microgrooves.

The present study deals with the development of a FMHP concept to be used for cooling high power dissipation electronic components. First, a state of the art concerning technologies, testing, and modeling aspects of the two-phase cooling systems (micro heat pipes, mini heat pipes, and mini heat spreaders) is presented. Then, experiments are carried out in order to determine the thermal performance of a FMHP as a function of various parameters such as the heat input power, the tilt angle, and the heat sink temperature. A mathematical model of a FMHP with axial rectangular microchannels is developed in which the fluid flow is considered along with the heat and mass transfer processes during evaporation and condensation. The numerical simulation results are presented regarding the thickness distribution of the liquid film in a microchannel, the liquid and vapor pressures and velocities as well as the wall temperatures along the FMHP. By comparing the experimental results with numerical simulation results, the reliability of the numerical model can be verified.

II. Literature Survey on Micro/Mini Heat Pipe Prototyping and Testing

A. Micro Heat Pipes

The earliest developments of micro heat pipes consisted of a long thin noncircular channel that utilizes sharp-angled corner regions as liquid arteries. Different micro heat pipes of different shapes are studied in open literature (Fig. 1). The triangular shape (Fig. 1.a) has been proposed for the first time by Cotter [2] in a theoretical study related to the determination of the maximum heat transfer capacity of individual microchannels. The rectangular shape with straight sides (Fig. 1.b) or incurved sides (Fig. 1.h), and the square shape with straight sides (Fig. 1.c) are studied by Itoh and Polasek [3] and Ji et *al.* [4]. The trapezoidal shape (Fig. 1.e) has been studied experimentally by Babin et *al.* [5,6], Wu and Peterson [7], and Wu et *al.* [8]. The circular shape with incurved walls (Fig. 1.f) has been studied by Ji et *al.* [4]. The microchannel having a triangular cross section with concave walls (Fig. 1.g) has been tested by Moon et *al.* [9]. It was apparent that micro heat pipes function in nearly the same manner as conventional liquid artery heat pipes. The capillary pressure difference insures the flow of the working fluid from the condenser back to the evaporator through the triangular-shaped corner regions. These corner regions serve as liquid arteries, thus no wicking structure is required.

Shapes with straight walls

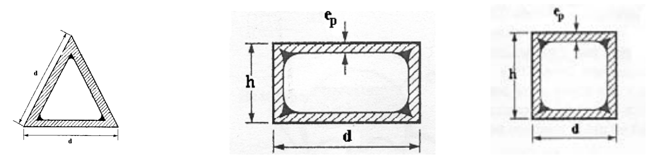

(a) Triangular section (b) Rectangular section (c) Square section

Shapes with incurved walls

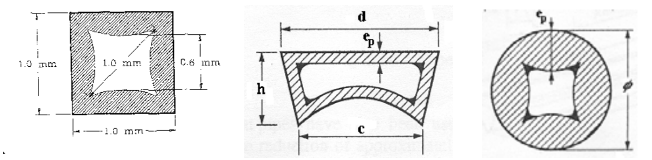

(d) Square section (e) Trapezoidal section (f) Circular section

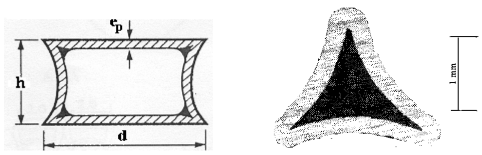

(h) Rectangular section (g) Triangular section

Fig.1. Cross sections of individual microchannels

Although the micro heat pipes show good thermal performances, several issues have not been addressed. These include mainly the determination of the effect of the precise size and shape of the micro heat pipe, and performance degradation with respect to time.

The experimental investigations on the individual micro heat pipes have included both steady-state and transient investigations. The results of these tests indicated the following important results:

(i) The micro heat pipes have been shown to be effective in dissipating and transporting heat from localized heat sources,
(ii) The maximum heat transport capacity is mainly dependent upon the adiabatic vapor temperature,
(iii) The shape and the number of the corner regions that serve as liquid arteries affect considerably the thermal performances of such devices,
(iv) The fill charge, that is the fluid amount to be introduced within the individual micro heat pipe, plays an important role in the degradation of the maximum heat transport. Thus, the liquid quantity has to be optimized in accordance to the operating conditions,
(v) The wall thickness of the individual micro heat pipes has a greater effect on the thermal performance than the casing material.

B. Silicon Flat Mini Heat Pipes and Mini Heat Spreaders

Researches related to the determination of the thermal performances of flat mini heat pipes (FMHPs) and flat mini heat spreaders (FMHS), which have capillary structures composed of microchannels, can be classified in two categories according to the used materials. Thus, we distinguish those manufactured in silicon and those made of materials such as copper, aluminum, and brass.

For silicon FMHPs, the basis for the fabrication include the use of conventional techniques such as the machining of small channels [10, 11], the use of directionally dependent etching processes to create rectangular or triangular-shaped channels [10, 12-32], or other more elaborate techniques that utilize a vapor deposition process [33-37] to create an array of long narrow channels of triangular cross section lined with a thin layer of copper. In this latter process, the copper lining on the inside of the channels eliminates the possibility of migration of the working fluid throughout the semiconductor material. Other techniques were considered: wafer sawing [15, 18-20, 38], anisotropic etching [39-44], Photolithography [45-48], and plasma etching [18-19, 49-50].

A literature survey of the micromachining techniques and capillary structures that have been used in silicon materials are reported in table 1. It can be concluded that two kinds of silicon two-phase cooling systems are considered:

(i) Silicon FMHPs with arrays of axial microgrooves [10, 12-16, 18-19, 21-37, 39-44, 49, 51-52] or radial ones [45-47].
(ii) Silicon FMHS acting as heat spreaders [17-20, 38].

The most important aspects of the FMHPs with arrays of axial microgrooves are the shape and the areas of the liquid and vapor passages. A number of investigations have been carried out in order to optimize the microgrooves and their liquid charge. Indeed, the experimental studies show that arrays of microgrooves are extremely sensitive to flooding, and for this reason several different charging methods have been developed. These vary from those that are similar to the methods used on conventional heat pipes to a method in which the working fluid is introduced and then the wafer is heated to above the critical temperature of the working fluid so that the working fluid in the supercritical state spreads entirely as a vapor, and uniformly distributed throughout the individual microgrooves. The array is then sealed and cooled below the critical temperature, allowing the vapor to cool and condense.

The FMHPs with arrays of microgrooves are able to improve the effective thermal conductivity. However, the heat transfer enhancement is limited since they only provide heat transfer along the axial direction of the individual arrays of microgrooves. To overcome this limitation, flat mini heat spreaders capable of distributing heat over a two-dimensional surface are proposed and tested. The results of the tests have demonstrated that heat spreaders allow the heat to be dissipated in any direction across the silicon wafer surface, thereby improving the thermal performances. The resulting effective thermal conductivities can approach and in some cases exceed those of diamond coatings of equivalent thickness. However, several aspects of the technology remain to be examined, but it is clear from the results of the experiment tests that heat spreaders fabricated as integral parts of silicon chips, present a feasible alternative cooling scheme that merits serious consideration for a number of heat transfer applications such as electronics cooling. Indeed, the heat spreaders could significantly decrease the temperature gradient across the chip, decrease the

TABLE I
OVERVIEW OF THE MICROMACHINING TECHNIQUES OF MICROGROOVES FOR SILICON FMHPS

Author	Technique	Capillary structure
Peterson [10]	Machining	Triangular axial grooves
Gerner [12]	Orientation-dependent etching	Triangular axial grooves
Mallik and Peterson [13]	Orientation-dependent etching	Rectangular axial grooves
Mallik et *al.* [33]	Vapor deposition process	Triangular axial grooves
Peterson et *al.* [11]	Machining and ultraviolet bonding process	Rectangular axial grooves
Gerner et *al.* [12]	Orientation-dependent etching	Triangular axial grooves
Mallik et *al.* [34]	Vapor deposition process	Triangular axial grooves
Peterson et *al.* [15]	Machining with a micro automation silicon dicing saw	Rectangular axial grooves
	Orientation-dependent etching	V-shaped axial grooves
Weichold et *al.* [35]	Vapor deposition process	V-shaped axial grooves
Adkins et *al.* [38]	Silicon dicing saw	Wick pattern
Gerner et *al.* [16]	Orientation-dependent etching	Triangular axial grooves
Peterson and Mallik [36,37]	Vapor deposition process	V-shaped axial grooves
Shen et *al.* [17]	Orientation-dependent etching	Cubic wick patter
Benson et *al.* [18,19]	Bidirectional saw cuts	Wick pattern
	Orientation-dependent etching	Triangular axial grooves
	Photomask and plasma etching	Wick pattern
Badran et *al.* [21]	Orientation-dependent etching	Triangular axial grooves
Benson et *al.* [20]	Bidirectional saw cuts	Wick pattern
Gromoll [22]	Orientation-dependent etching	Pyramidal wick pattern
Avenas et *al.* [23]	Orientation-dependent wet etching and bonding	Rectangular axial grooves
Avenas et *al.* [24]	Orientation-dependent wet etching and bonding	Rectangular axial grooves
Gillot et *al.* [25]	Orientation-dependent wet etching and bonding	Rectangular axial grooves
Kalahasti and Joshi [45]	Photolithography and Ni-electrodepositing	Radially diverging double wick pattern
Kang et *al.* [46]	Photolithography wet etching and bounding	Radial trapezoidal grooves
Kang and Huang [47]	Photolithography wet etching and bounding	Radial Star and rhombus grooves
Perret et *al.* [49]	Plasma etching and bounding	Rectangular axial grooves
Gillot et *al.* [26,27]	Orientation-dependent wet etching and bonding	Rectangular axial grooves
Ivanova et *al.* [29]	Etching and bonding	Rectangular axial grooves
Launay et *al.* [40]	Anisotropic etching process and bounding	Triangular axial grooves
Le Berre et *al.* [39]	Anisotropic etching process and bounding	Triangular axial grooves
Lee et *al.* [30,31]	Orientation-dependent wet etching	Triangular axial grooves
Murphy et *al.* [51]	—[a]	Rectangular axial grooves
Gillot et *al.* [28]	Orientation-dependent wet etching and bonding	Rectangular axial grooves
Laï et *al.* [32]	Orientation-dependent wet etching and bonding	Rectangular axial grooves
Launay et *al.* [41]	Anisotropic etching process and bonding	Triangular axial grooves
Murphy et *al.* [52]	—[a]	Rectangular axial grooves
Ivanova et al. [50]	Plasma etching	Hexagonal pins in the evaporator zone, radial grooves in the adiabatic section, and rectangular grooves in the adiabatic zone
Le Berre et al. [42]	Anisotropic etching process and bonding	Triangular axial grooves
Pandraud et al. [43]	Anisotropic etching process and bonding	Triangular axial grooves
Harris et al. [44]	Anisotropic etching process and bonding	Square axial grooves
Kang et al. [48]	Lithography and anodic bonding process	Triangular axial grooves

[a] Not specified in the reference

localized hot spots, and thereby improving the wafer reliability. In addition to reducing maximum chip temperature and increasing effective thermal conductivity, the heat spreaders can significantly improve the transient thermal response of the wafers. Finally, several new designs have been and continue to be developed in order to optimize wicking structures and new fabrication technologies.

C. Metallic Flat Mini Heat Pipes and Mini Heat Spreaders

For the metallic FMHPs, the fabrication of microgrooves on the heat pipe housing for the wick structure has been widely adopted as means of minimizing the size of the cooling device. Hence, FMHPs include axial microgrooves with triangular, rectangular, and trapezoidal shapes (Figure 2). Investigations into FMHPs with newer groove designs have also been carried out, and recent researches include triangular grooves coupled with arteries, star and rhombus grooves, microgrooves mixed with screen mesh or sintered metal. The fabrication of narrow grooves with sharp corner angle is a challenging task for conventional micromachining techniques such as precision mechanical machining. Accordingly, a number of different techniques including high speed dicing and rolling method [53], Electric-Discharge-Machining (EDM) [54-56], CNC milling process [55, 57-60], drawing and extrusion processes [62-64], metal forming process [65-68], and flattening [69] have been applied to the fabrication of microgrooves. More recently, laser-assisted wet etching technique was used in order to machine fan-shaped microgrooves [70]. A literature survey of the micromachining techniques and capillary structures that have been used in metallic materials are reported in table 2.

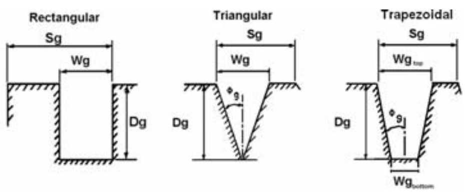

Fig. 2. Geometrical parameters of the groove shapes

It can be seen from this overview that three types of grooved metallic FMHP are developed:

(i) Type I: FMHPs with only axial rectangular, triangular or trapezoidal grooves [23, 53-56, 58, 60-79]. These FMHPs allow for high heat fluxes for horizontal or thermosyphon positions (up to 150 W/cm²). However, in the majority of the cases, the thermal performances of such FMHPs don't meet the electronic cooling requirements when the anti-gravity position is requested since the FMHP thermal performances are greatly altered for these conditions because the standard capillary grooves are not able to allow for the necessary capillary pumping able to overcome the pressure losses.

(ii) Type II: FMHPs with mixed capillary structures such as grooves and sintered metal powder or grooves and screen meshes [59, 65-66, 77-78]. Depending on the characteristics of the capillary structures such as the pore diameter, the wire diameter, the wire spacing and the number for screen wick layers, these FMHPs could meet the electronic cooling requirements especially for those applications where the electronic devices are submitted to forces such as gravity, acceleration and vibration forces [80]. However, for standard applications, these FMHPs allow for low thermal performances (lower heat fluxes and higher thermal resistance) when compared to those delivered by the FMHPs of Type I.

(iii) Type III: wickless FMHPs [55, 57]. These FMHPs utilize the concept of the boiling heat transfer mechanism in narrow space, and can remove high heat flux rates with great temperature gradient between the hot source and the cold one.

From the studies published in open literature, the following points can be outlined:

(i) The importance of the choice of the microchannel geometry. Indeed, according to the shape of a corner, the capillary pressure generated by the variation of the liquid-vapor interface curvature between the evaporator and the condenser, can be improved. An optimal shape of a corner permits to supply efficiently the evaporation zone in liquid, so that more heat power can be dissipated, and dry-out, which causes heat transfer degradation, can be avoided.

(ii) The choice and the quantity of the introduced fluid in the microchannel play a primordial role for the good operation of the FMHP.

(iii) Although the heat flux rates transferred by FMHP with integrated capillary structure are low, these devices permit to transfer very important heat fluxes avoiding the formation of hot spots. Their major advantage resides in their small dimensions that permit to integrate them near the heat sources.

The effect of the main parameters, of which depends the FMHP operation, can be determined by a theoretical study. Hence, the influence of the liquid and vapor flow interaction, the fill charge, the contact angle, the geometry, and the hydraulic diameter of the microchannel can be predicted by analyzing the hydrodynamic and thermal aspects.

III. Literature Survey on Micro/Mini Heat Pipe Modeling

The theoretical studies permit to predict the thermal performance of the FMHPs and their limits of operation according to the geometrical parameters, the thermophysical properties of the fluid and the wall, the fluid charge, the contact angle, the inertia forces, and the imposed boundary conditions (the dissipated heat flux rate and the cooling fluid temperature). The theoretical studies are important for understanding the FMHP operation because some phenomena are sometimes delicate to observe by experimental way.

Most of the theoretical models, which are proposed in the literature, are established for tubular heat pipes including straight or helicoidal axial grooves [81-82], and it is difficult to transpose them to the case of FMHPs because several interfacial phenomena are not considered in such models.

A. Micro Heat Pipes

Theoretical models have been developed in order to predict the thermal performance of such microchannels. Thus, Cotter [2], Babin et *al.* [5-6], Gerner et *al.* [14], Duncan and Peterson [83], Khrustalev and Faghri [84], Longtin et *al.* [85] Peterson and Ma [86], Zaghdoudi et *al.* [87], Ha and Peterson [88], Ma and Peterson [89], , Sobhan et *al.* [90], Do et *al.* [91],

TABLE II
OVERVIEW OF THE MICROMACHINING TECHNIQUES OF MICROGROOVES FOR METALLIC FMHPS

Author	Micromachining Technique	Material	Capillary structure
Murakami et *al.* [71]	__[a]	Brass	Triangular and rectangular grooves
Plesh et *al.* [72]	__[a]	Copper	Axial and transverse rectangular grooves
Sun and Wang [73]	__[a]	Aluminum	V-shaped axial grooves
Ogushi and Yamanaka [74]	__[a]	Brass	Triangular and trapezoidal axial grooves
Cao et *al.* [54]	Electric-discharge-machining (EDM)	Copper	Rectangular axial grooves
Hopkins et *al.* [53]	Rolling method High-speed dicing saw	Copper	Trapezoidal diagonal grooves Rectangular axial grooves
Schneider et *al.* [65-67]	Metal forming process	AlSiC	Triangular axial grooves
Avenas et *al.* [23]	__[a]	Brass	Rectangular axial grooves
Zaghdoudi and Sarno [80]	Milling process and sintering	Copper	Rectangular axial grooves and sintered powder wick
Cao and Gao [55]	Milling process Electric Discharge Machining (EDM)	Aluminum Copper	Perpendicular network of crossed grooves Triangular axial grooves
Lin et *al.* [56]	Electric-discharge-machining (EDM)	Copper	Rectangular axial grooves
Chien et *al.* [68]	Metal forming process	Aluminum	Radial rectangular grooves
Gao and Cao [57]	Milling process	Aluminum	Waffle-like cubes (protrusions)
Moon et *al.* [61]	Drawing and extrusion process	Copper	Triangular and rectangular axial grooves with curved walls
Soo Yong and Joon Hong [75]	__[a]	__[a]	Rectangular axial grooves with half circle shape at the bottom
Lin et *al.* [58]	Etching, CNC milling, and sintering	Copper	Radial diverging grooves and sintered powder wick
Moon et *al.* [62]	Drawing process	Copper	Triangular and rectangular grooves with incurved walls
Romestant et *al.* [63]	Extrusion	Aluminum	Triangular axial grooves
Zaghdoudi et *al.* [59]	Milling process	Copper	Triangular axial grooves and meshes
Zhang et *al.* [76]	__[a]	Copper Stainless steel Copper	Rectangular axial grooves Trapezoidal axial grooves
Iavona et *al.* [50]	Direct Bounded Copper technology	Copper/Alumina	Fiber mixed material of Al_2O_3 and SiO_2
Popova et *al.* [77]	__[a]	Copper	Rectangular grooves machined in sintered copper structure
Popova et *al.* [78]	__[a]	Copper	Rectangular grooves machined in sintered copper structure
Lefèvre et *al.* [60]	Milling process	Copper	Rectangular axial grooves
Lim et *al.* [70]	Laser micromachining	Copper	Triangular axial grooves with curved walls
Tao et *al.* [69]	Flattening of cylindrical finned tubes	Copper	Rectangular axial grooves with half circle shape at the bottom
Zhang et *al.* [79]	__[a]	Copper	Radial diverging grooves
Xiaowu et *al.* [64]	Extrusion-ploughing process	__[a]	V-shaped grooves

[a] Not specified in the reference

Suman et *al.* [92], Suman and Kumar [93], and Hung and Seng [94] developed theoretical one dimensional models that analyze the liquid and vapor flow along microchannels in steady state regime. These models consist of solving the equations of mass, momentum and energy conservation applied to each of the liquid and vapor phase. Such models permit to predict, from the capillary limit, the maximum heat power transported by a microchannel and the optimum quantity of the fluid to be introduced. To determine the temperature field, it is necessary to consider the diffusion equation in wall.

The one-dimensional models of liquid-vapor flow are developed for microchannels with different cross sections. The obtained differential equations are first order, coupled and nonlinear equations. The numerical solution of the problem permits to determine the axial flow parameters such as the liquid and vapor pressure distributions, and the vapor and the liquid velocities along the microchannel. The model output includes also the variation of the liquid-vapor radius of curvature in the direction of the flow. The liquid and vapor sections, the interfacial area, and the contact area of the liquid and vapor phases with the walls are expressed as a function of the contact angle and the radius of curvature of the liquid-vapor interface. Nevertheless, these models don't include the heat transfer analysis in the evaporator and condenser zones, and the temperature distribution along the microchannel cannot be predicted.

To determine the condenser and evaporator heat transfer coefficients, the simplest method consists to consider only the heat transfer by conduction through the liquid film if we neglect the interfacial thermal resistance. Generally, in the evaporator and the condenser, two zones are considered: a zone with a constant liquid-vapor radius of curvature, and a zone, near to the wall, with a variable radius of curvature [84]. Many researches, which were carried out on the liquid-wall contact zone (clash zone), showed that it is necessary to take into account the thermal transfer in this region in the evaporator and, also, in the condenser sides. Indeed, in the evaporator and in the condenser, it is necessary to consider various zones of the meniscus. Wayner et *al.* [95] showed that, in the clash zone, the curvature of the interface is not constant, and the liquid-vapor interface temperature is different from the temperature of saturation. Three zones are considered: a zone of very small thickness where the fluid is adsorbed on the wall in equilibrium phase, a zone where the curvature radius is variable (microregion) and a zone where the curvature radius is constant (macroregion). Many studies [96-101] were developed to solve this problem numerically. In these studies, the models of microregion and macroregion don't consider the axial flow along the microchannel.

The micro heat pipe models lead to the following main conclusions:

- The analytical models developed have been shown to predict the steady-state performance limitations and operational characteristics with a reasonable degree of accuracy. The perceived accuracy of the models is strongly dependent upon the way dry-out is defined. To resolve this problem, it is necessary to understand the dry-out phenomenon better and define more clearly when it begins and how it proceeds.
- The maximum heat transport corresponds to the capillary limit, which is found to be the operating limit for most micro heat pipes.
- When the working temperature of the micro heat pipe raises, the heat transport capability increases.
- The heat transport capability of the micro heat pipe is relevant to the tilt angles, but only has a little effect.
- It is demonstrated that the optimal charge value would not exceed 25% even for heat input power levels near zero.
- Shear stresses in the liquid at the liquid-vapor interface due to frictional interaction significantly influence the maximum heat transport capacity, and increase the length of the liquid blocking zone in the condenser.
- The dynamic component of the pressure gradient in the liquid has no pronounced effect on the performance characteristics of the micro heat pipe, and for nearly maximum heat loads, the largest portion of the liquid pressure drop occurred in the evaporator and the beginning of the adiabatic section, where the liquid cross-sectional area is several times smaller than that in the condenser.
- The dominant thermal resistances within the micro heat pipes are those of vapor flow and the liquid film in the evaporator and condenser.
- The amount of working fluid and the minimum wetting contact angle strongly influence the performance characteristics of the micro heat pipe.
- There exists an optimum hydraulic radius for the grooves that have a maximum capillary heat transport capability, and when the hydraulic radius is less than the optimum hydraulic radius, the groove dimension will directly limit the capillary heat transport capability. Also, when the hydraulic radius of the cross section of the grooves is much larger than the optimum hydraulic radius, no increase in the capillary pumping occurs.
- The use of star-groove family shape provides a desired corner apex angle without affecting the number of corners of the micro heat pipe. Under identical operating conditions, the comparisons of performance between star-groove family and regular polygonal micro heat pipe reveal that the former outperforms the latter by virtue of its flexibility in reducing the corner apex angle for providing higher capillarity. With the corner apex angle being held constant, it is found that the performance of a micro heat pipe deteriorates with increase in number of corners. Moreover, it is observed that heat transport capacity increases with cross-sectional area of the micro heat pipe.
- The increase in the total length of the micro heat pipe results in decrease in its heat transport capacity. However, the heat transport capacity increases when the adiabatic section length is decreased with the total length being fixed.

B. Flat Mini Heat Pipes

For FMHPs constituted of an integrated capillary structure including microchannels of different shapes and associated in network, the theoretical approach consists of studying the flow and the heat transfer in isolated microchannels.

Khrustalev and Faghri [100] developed a detailed mathematical model of low-temperature axially grooved FMHP in which the fluid circulation is considered along with the heat and mass transfer processes during evaporation and condensation. The results obtained are compared to existing experimental data. Both capillary and boiling limitations are found to be important for the flat miniature copper-water heat pipes, which is capable of withstanding heat fluxes on the order of 40 W/cm² applied to the evaporator wall in the vertical position. The influence of the geometry of the grooved surface on the maximum heat transfer capacity of the miniature heat pipe is demonstrated.

Faghri and Khrustalev [102] studied an enhanced flat miniature heat pipe with capillary grooves for electronics cooling systems have. They survey advances in modeling of important steady-state performance characteristics of enhanced and conventional flat miniature axially-grooved heat pipes such as the maximum heat flow rate, thermal resistance of the evaporator, incipience of the nucleate boiling, and the maximum heat flux on the evaporator wall.

Khrustalev and Faghri [103] analyze friction factor coefficients for liquid flow in a rectangular microgroove coupled with the vapor flow in a vapor channel of a miniature two-phase device. The results show that the effect of the vapor-liquid frictional interaction on the liquid flow decreases with curvature of the liquid-vapor interface. Shear stresses at the liquid-vapor interface are significantly non-uniform, decreasing towards the center of the liquid-vapor meniscus.

Lefevre et *al.* [104] developed a capillary two-phase flow model of flat mini heat pipes with micro grooves of different cross-sections. The model permits to calculate the maximum heat transfer capabilities and the optimal liquid charge of the FMHP. The results are obtained for trapezoidal and rectangular micro grooves cross-sections.

Launay et *al.* [105] developed a detailed mathematical model for predicting the heat transport capability and the temperature distribution along the axial direction of a flat miniature heat pipe, filled with water. This steady-state model combines hydrodynamic flow equations with heat transfer equations in both the condensing and evaporating thin films. The velocity, pressure, and temperature distributions in the vapor and liquid phases are calculated. Various boundary conditions fixed to the evaporator and condenser have been simulated to study the thermal performance of the FMHP below and above the capillary limit. The effect of the dry-out or flooding phenomena on the FMHP performance, according to boundary conditions and fluid fill charge, were also predicted.

Tzanova et *al.* [106] presented a detailed analysis on maximum heat transfer capabilities of silicon-water FMHPs. The predictive hydraulic and thermal models were developed to define the heat spreader thermal performances and capillary limitations. Theoretical results of the maximal heat flux that could be transferred agreed reasonably well with the experimental data and the developed model provides a better understanding of the heat transfer capability of FMHPs.

Angelov et *al.* [107] proposed theoretical and modeling issues of FMHPs with parallelepipedal shape with regard to the capillary limit and the evaporator boiling limit. An improved model is suggested and it is compared with the simulation and experimental results. The improved model implements a different analytically derived form of the friction factor-Reynolds number product. The simulated results with the proposed model demonstrate better coherence to the experiment showing the importance of accurate physical modeling to heat conduction behavior of the FMHP.

Shi et *al.* [108] carried out a performance evaluation of miniature heat pipes in LTCC by numerical analysis, and the optimum miniature heat pipe design was defined. The effect of the groove depth, width and vapor space on the heat transfer capacity of miniature heat pipes was analyzed.

Do et al. [109] developed a mathematical model for predicting the thermal performance of a FMHP with a rectangular grooved wick structure. The effects of the liquid-vapor interfacial shear stress, the contact angle, and the amount of liquid charge are accounted for in the model. In particular, the axial variations of the wall temperature and the evaporation and condensation rates are considered by solving the one-dimensional conduction equation for the wall and the Young-Laplace equation, respectively. The results obtained from the proposed model are in close agreement with several existing experimental data in terms of the wall temperatures and the maximum heat transport rate. From the validated model, it is found that the assumptions employed in previous studies may lead to significant errors for predicting the thermal performance of the heat pipe. Finally, the maximum heat transport rate of a FMHP with a grooved wick structure is optimized with respect to the width and the height of the groove by using the proposed model. The maximum heat transport rate for the optimum conditions is enhanced by approximately 20%, compared to existing experimental results.

Do and Jang [110] investigated the effect of water-based Al2O3 nanofluids as working fluid on the thermal performance of a FMHP with a rectangular grooved wick. For the purpose, the axial variations of the wall temperature, the evaporation and condensation rates are considered by solving the one-dimensional conduction equation for the wall and the Young-Laplace equation for the phase change process. In particular, the thermophysical properties of nanofluids as well as the surface characteristics formed by nanoparticles such as a thin porous coating are considered. From the comparison of the thermal performance using both water and nanofluids, it is found that the thin porous coating layer formed by nanoparticles suspended in nanofluids is a key effect of the heat transfer enhancement for the heat pipe using nanofluids. Also, the effects of the volume fraction and the size of nanoparticles on the thermal performance are studied. The results show the feasibility of enhancing the thermal performance up to 100% although water-based Al2O3 nanofluids with the concentration less than 10% is used as working fluid. Finally, it is shown that the thermal resistance of the nanofluid heat pipe tends to decrease with increasing the nanoparticle size, which corresponds to the previous experimental results.

From the FMHP models, the following main conclusions can be outlined:

- An increase of the heat load decreases the evaporator thermal resistance and increases the condenser thermal resistance due to the change in the longitudinal meniscus distribution along the FMHP.
- Shear stresses at the liquid-vapor interface are significantly non-uniform, decreasing towards the center of the liquid-vapor meniscus. This non uniformity increases with curvature of the liquid-vapor interface.
- The effect of the vapor flow on the liquid flow in the grooves decreases with curvature of the liquid-vapor interface.
- Frictional vapor-liquid interaction significantly affects the thermal performance of the FMHP with axial grooves, and shapes of the liquid and vapor cross-sectional areas should be precisely accounted for when calculating the friction factor-Reynolds number products.
- At the evaporator, heat is mainly transferred in the short thin film region, where the liquid is very close to the wall. It results from the effect of the adhesion forces on the meniscus curvature and from the capillary forces and from the capillary forces. Thus, to improve heat transfer, the microregion number in a FMHP cross section must be as high as possible.
- For triangular microchannels, the heat transfer rate is rather limited by the large pressure drops in the corners; nevertheless, the vapor pressure drops are not negligible.
- The thermal resistance of the vapor phase is more important than the transversal thermal resistance in the liquid film and the wall. Thus, increasing the triangular cross-section allows the increase of the liquid and vapor flow cross sections, and consequently the increase of the capillary limit and the reduction of the vapor thermal resistance.

- The thermal performances of the FMHP are strongly dependent on the amount of working fluid: a too large amount leads to condenser flooding, and a too small amount leads to evaporator dry-out. In both cases, the heat transfer areas are reduced, and the liquid thermal resistance increases.
- The assumptions that evaporation and condensation occur uniformly in the axial direction, that evaporation occurs only in the evaporator section, and that condensation occurs only in the condenser section, are valid only if the axial wall conduction can be neglected.
- As the amount of liquid charge increases, the maximum capillary limit increases modestly due to a decrease in the effective heat pipe length, but the thermal resistance increases much more rapidly.

C. Flat Mini Heat Spreaders

For the mini heat spreaders (FMHS), the modeling approach is quite different. Indeed, two or three-dimensional models for thermal transport in heat pipes are considered. The capillary structure is modeled by considering a porous medium. Through the permeability and the equivalent thermal conductivity of the porous medium, lots of capillary structures can be modeled. Thin models account for fluid flow in the liquid phase, vapor phases and the wicks, heat conduction in the wall, heat and mass transfer at the vapor-wick interface.

Wang and Vafai [111] developed analytical models for predicting the transient performance of a FMHS for startup and shutdown operations. These models can be utilized separately for a startup or a shutdown operation, respectively. The two models can also be combined together to simulate the thermal performance of a FMHS in cyclical startup and shutdown operations. The transient temperature distributions in the FMHS walls and wicks are presented in this work. The results reveal that the thermal diffusivity, the thickness of the wall and the wick, and the heat input pattern affect the heat pipe time constants. The wicks create the main thermal resistance resulting in the largest temperature drop in the FMHS, thus substantially influencing its performance.

Kalahasti and Joshi [45] conducted a combined numerical and experimental investigation on a novel FMHS, to better understand the effect of primary operating parameters governing the performance of such devices. A numerical thermal model was developed to predict the temperature response with variation in the leading geometrical, material and boundary parameters of the spreader versus wall thickness, thermal conductivity, power input and heat source size. The results showed that, unlike conventional heat pipes, wall thermal conductivity is a major factor in such thin, flat spreaders. The spreader performance also degrades with decrease in heat source size. Visualization experiments have been conducted to qualitatively understand the heat transfer phenomena taking place on these devices. These confirmed that the primary limitation to heat transfer from these devices was due to the capillary limitation of the wick structures.

Vadekkan et *al.* [112] developed a three-dimensional to analyze the transient and steady-state performance of FMHS subjected to heating with multiple discrete heat sources. Three-dimensional flow and energy equations are solved in the vapor and liquid regions, along with conduction in the wall. Saturated flow models are used for heat transfer and fluid flow through the wick. Predictions are made for the magnitude of heat flux at which dry-out would occur in a FMHS. The input heat flux and the spacing between the discrete heat sources are studied as parameters. The location in the FMHS at which dry-out is initiated is found to be different from that of the maximum temperature. The location where the maximum capillary pressure head is realized also changes during the transient. Axial conduction through the wall and wick are seen to play a significant role in determining the axial temperature variation.

Kamenova et *al.* [113] developed 2D hydraulic model in order to analyze the fluid flow and heat and mass transfer in a thin heat spreader including sintered copper wick structure. Further, according to the real prototype and the experimental setup, the simplified model was developed in more detailed formulation. The results are presented in terms of liquid and vapor pressures within the FMHS and maximal heat power. Experimental validation, which proves that the new model can be used to predict the heat capacity and to improve the design of FMHS for specific applications, is also presented.

Lefèvre and Lallemand [114] developed a 3D analytical solution for both the liquid and vapor flows inside a heat spreader coupled to an analytical solution for the temperature. The maximum heat transfer capability of a FMHS, on which several heat sources and heat sinks are located, is calculated. The capillary structure inside the FMHS is modeled by considering a porous medium, which allows to take into account capillary structures such as meshes or sintered powder wicks. The thermal model is able to calculate the part of heat flux transferred only by heat conduction in the FMHS wall from the heat transferred by change of phase.

Koito et *al.* [115] carried out a numerical analysis on a FMHS called "vapor chamber". The vapor chamber is an advanced cooling heat spreader for high-performance microchips, such as new generation CPUs in personal computers and workstations. The mathematical model of the vapor chamber formulated in this study is a two-phase closed disk-shaped chamber and is placed between a small heat source and a large heat sink. Wick sheets and a wick column are provided inside the vapor chamber to circulate the working fluid. By solving the equations of continuity, momentum and energy numerically, the velocity, pressure and temperature distributions inside the vapor chamber are obtained. From the numerical results, the capillary pressure head necessary to circulate the working fluid is estimated and the temperature drop inside the vapor chamber is determined. These numerical results are useful for the design and improvement of the vapor chamber.

El-Genk et *al.* [116] investigated the performance of composite spreaders consisting of a layer of porous graphite and a copper substrate. The analysis solves the three-dimensional heat conduction equations in both the graphite and copper substrates.

Sonan et *al.* [117] studied theoretically the transient performance of a flat heat spreader used to cool multiple electronics components. The fluid flows in both wick and vapor core were computed using a transient 2D hydrodynamic model. This model was coupled with a transient 3D thermal model of the FMHS wall, designed to calculate the heat transfer through the wall. An interesting procedure for solving the governing equations for the heat and mass transfers inside the heat spreader is proposed. The phase change mechanisms at the liquid-vapor interface are included in this procedure through the Clausius-Clapeyron law. During a start-up, the transient model is able to predict the velocity and pressure distribution of the liquid and the vapor, and thus the transient response of the heat spreader.

Xiao and Faghri [118] developed a detailed, three-dimensional in order to analyze the thermal hydrodynamic behaviors of FMHS without empirical correlations. The model accounts for the heat conduction in the wall, fluid flow in the vapor chambers and porous wicks, and the coupled heat and mass transfer at the liquid/vapor interface. The FMHS with and without vertical wick columns in the vapor channel are intensively investigated in the model. Parametric effects, including evaporative heat input and size on the thermal and hydrodynamic behavior in the FMHS, are investigated. The results show that, the vertical wick columns in the vapor core can improve the thermal and hydrodynamic performance of the FMHS, including thermal resistance, capillary limit, wall temperature, pressure drop, and fluid velocities due to the enhancement of the fluid/heat mechanism from the bottom condenser to the top evaporator. The results predict that higher evaporative heat input improves the thermal and hydrodynamic performance of the FMHS, and shortening its size degrades its thermal performance.

Zhang et *al.* [79] developed a novel FMHS that can achieve more uniform heat flux distribution and thus enhance heat dissipation of heat sinks. The grooved structure of the FMHS can improve its axial and radial heat transfer and also can form the capillary loop between condensation and evaporation surfaces. A two-dimensional heat and mass transfer model for the grooved FMHS is developed. The numerical simulation results show that the thickness distribution of liquid film in the grooves is not uniform. The temperature and velocity field in the FMHS are obtained. The thickness of the liquid film in groove is mainly influenced by pressure of vapor and liquid beside liquid-vapor interface. The thin liquid film in heat source region can enhance the performance of the FMHS, but if the starting point of liquid film is backward beyond the heat source region, the FMHS will dry out easily. The optimal filling ratio should maintain steady thin liquid film in heat source region of the FMHS. The vapor condenses on whole condensation surface, so that the condensation surface achieves great uniform temperature distribution.

Ranjan et *al.* [119] developed a transient, three-dimensional model for thermal transport in a heat spreader. The Navier-Stockes equations along with the energy equation are solved numerically for the liquid-vapor and vapor flows. A porous medium formulation is used for the wick region. Evaporation and condensation at the liquid-vapor interface are modeled using kinetic theory.

From the theoretical studies on FMHS, the following conclusions can be outlined:

- The heat conduction through the FMHS wall can modify the maximum performance of a FMHS if the wall resistance is small enough.
- A higher evaporative heat input increases surface temperature, pressure drop, fluid velocities in the wicks and vapor chambers due to the increasing mass flow rate at the vapor-wick interface as vapor velocity increases.
- A larger FMHS has a better thermal performance than a smaller one because of the shortened evaporative heating area, although the vapor velocities increase caused by the increasing pressure when the size of the FMHS is shortened.

An overview of the main theoretical studies on micro heat pipes, mini heat pipes, and mini heat spreaders are listed in table 3.

TABLE III
OVERVIEW OF THE MAIN THEORETICAL STUDIES ON MICRO HEAT PIPES, MINI HEAT PIPES, AND MINI HEAT SPREADERS

Author	Capillary Structure
Micro Heat Pipes	
Cotter [2]	Triangular (three corner regions)
Babin et *al.* [5]	Square with incurved walls (four corner regions)
Babin et *al.* [6]	Square with incurved walls (four corner regions)
Gerner et *al.* [14]	Triangular (three corner regions)
Duncan and Peterson [83]	Triangular (three corner regions)
Khrustalev and Faghri [84]	Triangular (three corner regions)
Longtin et *al.* [85]	Triangular (three corner regions)
Peterson and Ma [86]	Triangular (three corner regions)
Zaghdoudi et *al.* [87]	Triangular (three corner regions)
Ha and Peterson [88]	Triangular (three corner regions)
Ma and Peterson [89]	Triangular (three corner regions)
Sobhan et *al.* [90]	Triangular (three corner regions)
Do et *al.* [91]	Triangular with incurved walls (three corner regions)
Suman et *al.* [92]	Triangular (three corner regions)
Suman and Kumar [93]	Polygonal (three and four corner regions)
Hung and Seng [94]	Square, hexagonal, octagonal star-grooves and equilateral triangle grooves
Flat Mini Heat Pipes	
Khrustalev and Faghri [100]	Rectangular axial grooves
Faghri and Khrustalev [102]	Rectangular axial grooves
Khrustalev and Faghri [103]	Rectangular axial grooves
Lefevre et *al.* [104]	Rectangular and trapezoidal axial grooves
Launay et *al.* [105]	Triangular axial grooves
Tzanova et *al.* [106]	Rectangular axial grooves
Angelov et *al.* [107]	Rectangular axial grooves
Shi et *al.* [108]	Rectangular axial grooves
Do et *al.* [109]	Rectangular axial grooves
Do and Jang [110]	Rectangular axial grooves
Flat Mini Heat Spreaders	
Wang and Vafai [111]	Porous medium
Kalahasti and Joshi [45]	Radial grooves
Vadakkan et *al.* [112]	Porous medium
Kamenova et *al.* [113]	Porous medium
Lefèvre and Lallemand [114]	Porous medium
Koito et *al.* [115]	Porous medium
El-Genk et *al.* [116]	Porous medium
Sonan et *al.* [117]	Porous medium
Xiao and Faghri [118]	Porous wick
Zhang et *al.* [79]	Radial grooves
Ranjan et *al.* [119]	Porous medium

IV. FMHP Fabrication and Experimental Study

A. FMHP Fabrication and Filling Procedures

A FMHP has been designed, manufactured, and tested. The design parameters are based on some electronic components that require high power dissipation rate. The design is subjected to some restrictions, such as the requirements for size, weight, thermal resistance, working temperature, and flow resistance. For comparison purposes, a solid heat sink that has the same size but more weight than the FMHP is also tested. The test sample is made of the same copper and their dimensions are 100 mm length, 50 mm width, and 3 mm thickness. The FMHP body is manufactured in two halves. Manufacturing of the FMHP begins with the capillary grooves being mechanically machined by a high speed dicing process in the first half (2 mm thick) and the second half, which consists of a copper cover slip 1 mm thick, is bonded to the first half by an electron beam welding process. The heat pipe charging tube (2 mm diameter), from which the fluid working is introduced, is bounded to the heat pipe end by a classic welding technique. The geometrical dimensions of the FMHPs are indicated in table 4 and in Fig. 3. A view of the microchannels is shown in Fig. 4.

Filling the FMHP presents one of the greatest challenges. In this study, a boiling method is used for the filling purpose. The filling assembly includes a vacuum system, a boiler filled with distilled water, vacuum tight electrovalves, a burette for a precise filling of the FMHP and a tubular adapter. The degassing and charging procedure consists of the following steps: (i) degassing water by boiling process, (ii) realizing a vacuum in the complete set-up, (iii) charging of the burette, and (iv) charging of the FMHP. An automatic process controls the whole steps. After charging the FMHP, the open end (a 2 mm diameter charging tube) is sealed. The amount of liquid is controlled by accurate balance. Indeed, the FMHP is weighed before and after the fill charging process and it is found that the optimum fill charge for the FMHP developed in this study is 1.2 ml.

B. Experimental Set-up and Procedures

Heat input is delivered by an electric resistance cartridge attached at one end of the FMHP and it is provided on the grooved side of the FMHP. The power input to the heater is controlled through a variable transformer so that a constant power is supplied to the heated section, and the voltage and current are measured using digital voltmeter and ammeter. Both the evaporator and the adiabatic sections are thermally insulated. The heat loss from the insulation surface to the ambient is determined by evaluating the temperature difference and the heat transfer coefficient of natural convection between the insulated outer surface and ambient. Heat is removed from the FMHP by a water cooling system. A thermally conductive paste is used to enhance the heat transfer between the copper FMHP and the aluminum blocks. The lengths of the evaporator, adiabatic, and condenser zones are L_e = 19 mm, L_a = 35 mm, and L_c = 45 mm, respectively. The temperature distribution across the surface of the FMHP and the copper plate is obtained using 6 type-J surface mounted thermocouples. The thermocouples are located, respectively at 5, 15, 27, 42, 60, and 90 mm from the end cap of the evaporator section. In order to measure the evaporator and condenser temperatures, grooves are practiced on the FMHP wall and thermocouples are inserted along the grooves. The thermocouples locations and the experimental set-up are shown in Figs. 5 and 6.

The experimental investigation focuses on the heat transfer characteristics of the FMHP at various heat flux rates, Q, and operating temperatures, T_{sf}. Input power is varied in increments from a low value to the power at which the evaporator temperature starts to increase rapidly. In the process, the temperature distribution of the heat pipe along the longitudinal axis is observed and recorded. All experimental data are obtained with a systematic and consistent methodology that is as follows. First, the flat miniature heat pipe is positioned in the proper orientation and a small heat load is applied to the evaporator section. Secondly, the heat sink operating temperature is obtained and maintained by adjusting the cooling water flow to the aluminum heat sink.

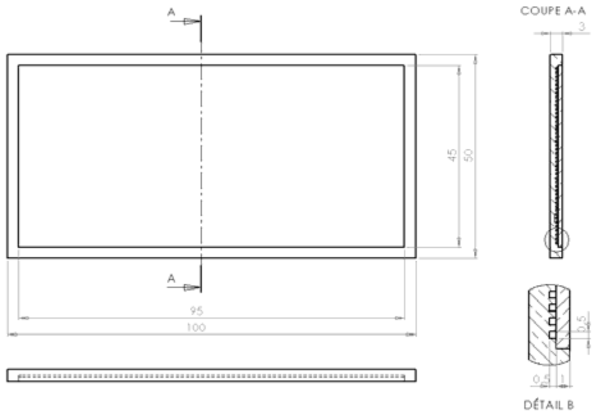

Fig. 3. Sketch of the FMHPs

Fig. 4. View of the microchannels

TABLE IV
MAIN GEOMETRICAL PARAMETERS OF THE FMHP

FMHP width, W	50
FMHP overall length, L_t	100
FMHP thickness, t	3
Microchannel height, D_g	0.5
Microchannel width W_g	0.5
Microchannel spacing S_g	1
Overall width of the microchannels	45
Overall length of the microchannels	95
Number of the microchannels, N_g	47

Dimensions are in mm.

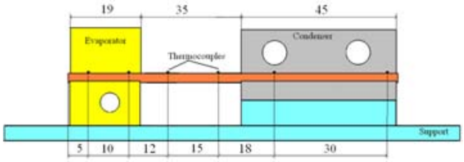

Fig. 5. Thermocouple locations

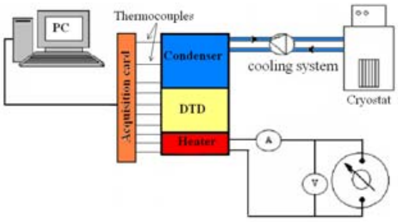

Fig. 6. Experimental set-up

Once the heat sink temperature is obtained, the system is allowed to reach steady-state over 10-15 minutes. After steady-state is reached, temperature readings at all thermocouples are recorded and power to the evaporator is increased by a small increment. This cycle is repeated until the maximum capillary limit is reached which is characterized by a sudden and steady rise of the evaporator temperature.

C. Measurement Uncertainty Analysis

The data logger TC-08 acquisition system is used to make all temperature measurements. The type J thermocouples are calibrated against a precision digital RTD and their accuracy over the range of interest is found to be within 0.5 °C. In the steady-state, the wall thermocouples fluctuate within 0.2 °C. The uncertainty of the thermocouples is $0.3°C + 0.03 \times 10^{-2}$ T, where T is the measured temperature. The uncertainty of the thermocouples locations is within 0.5 mm in the heat pipe axial direction. A pair of multimeters is used to determine and record the power supplied to the resistors. The first multimeter is used to measure voltage across the film resistor and has an accuracy of 2 % of true voltage while the second measures the AC current and has accuracy 2 % of true AC current.

The power input to the electric heater is calculated using the measured current and voltage ($Q = V \times I$). The thermal resistance, R_{th}, of the heat pipe is defined as the ratio of the temperature drop, $\Delta T = T_{ev} - T_c$, across the heat pipe to the input heat power Q. The uncertainty of the data is estimated as it follows.

The 95 percent confidence uncertainty on the thermal resistance, U_{Rth}, in the experimental result of R_{th}, is given by the combination of a precision contribution to the uncertainty of R_{th}, P_{Rth}, and a bias contribution to the uncertainty of R_{th}, B_{Rth}

$$U_{Rth} = \left[B_{Rth}^2 + P_{Rth}^2\right]^{1/2} \quad (1)$$

Since the heat pipe thermal resistance, R_{th}, is calculated from

$$R_{th} = \frac{\Delta T}{Q} = \frac{(T_{ev} - T_c)}{Q} \quad (2)$$

The precision and bias limits contributions can be evaluated separately in terms of the sensitivity coefficients of the result, R_{th}, to the measured quantities as

$$P_{Rth}^2 = \left(\frac{\partial R_{th}}{\partial T_{ev}}\right)^2 P_{Tev}^2 + \left(\frac{\partial R_{th}}{\partial T_c}\right)^2 P_{Tc}^2 + \left(\frac{\partial R_{th}}{\partial Q}\right)^2 P_Q^2 \quad (3)$$

$$B_{Rth}^2 = \left(\frac{\partial R_{th}}{\partial T_{ev}}\right)^2 B_{Tev}^2 + \left(\frac{\partial R_{th}}{\partial T_c}\right)^2 B_{Tc}^2 + \left(\frac{\partial R_{th}}{\partial Q}\right)^2 B_Q^2 + 2\left(\frac{\partial R_{th}}{\partial T_{ev}}\right)\left(\frac{\partial R_{th}}{\partial T_c}\right) B'_{Tc} B'_{Tev} \quad (4)$$

Where B'_{Tc} and B'_{Tev} are the portions of B_{Tc} and B_{Tev}, that arise from identical error sources (calibration errors of thermocouples that were calibrated using the same standards, equipment and procedures) and are therefore presumed to be perfectly correlated.

Using (2) to evaluate the derivatives, defining, $\Delta T = T_{ev} - T_c$ and rearranging, one obtains

$$\left(\frac{P_{Rth}}{R_{th}}\right)^2 = \left(\frac{P_{Tev}}{\Delta T}\right)^2 + \left(\frac{P_{Tc}}{\Delta T}\right)^2 + \left(\frac{P_Q}{Q}\right)^2 \quad (5)$$

$$\left(\frac{B_{Rth}}{R_{th}}\right)^2 = \left(\frac{B_{Tev}}{\Delta T}\right)^2 + \left(\frac{B_{Tc}}{\Delta T}\right)^2 + \left(\frac{B_Q}{Q}\right)^2 - 2\left(\frac{B'_{Tev}}{\Delta T}\right)\left(\frac{B'_{Tc}}{\Delta T}\right) \quad (6)$$

Where

$$\left(\frac{P_Q}{Q}\right)^2 = \left(\frac{P_V}{V}\right)^2 + \left(\frac{P_I}{I}\right)^2 \quad (7)$$

$$\left(\frac{B_Q}{Q}\right)^2 = \left(\frac{B_V}{V}\right)^2 + \left(\frac{B_I}{I}\right)^2 \quad (8)$$

V and I are the voltage and current values, respectively.

For calculating, the bias limit in R_{th} measurements, we suppose that the bias errors in the two temperature measurements are totally correlated. Note that in this case, the last term on the right side of (4) would cancel the first and the second terms and then B_{Rth}/R_{th} would be equal to B_Q/Q.

Table 5 gives the different values used and calculated in our uncertainty estimation. The calculated values of U_{Rth}/R_{th} obtained in our data for different input heat fluxes show that the highest uncertainty for R_{th} (up to 16%) occurs at lowest input power and it decreases with an increase in the input power.

TABLE V
VALUES CONSIDERED FOR UNCERTAINTY ESTIMATION

P_V/V	2 %
P_I/I	2 %
B_V/V	2 %
B_I/I	2 %
P_Q/Q	2.8 %
B_Q/Q	2.8 %
B_{Rth}/R_{th}	2.8 %

V. Experimental Results and Analysis

A. Combined Effects of the Heat Input Power and the Heat Sink Temperature

Fig. 7 illustrates typical steady temperature profiles for the FMHP prototypes for 10 W to 60 W at a heat sink temperature, T_{sf}, of 10 °C, 20 °C, and 40 °C, when it is oriented horizontally. The maximum evaporator temperature and temperature gradients for the FMHP are considerably smaller than those obtained for copper plate (Fig. 8). For instance, for T_{sf} = 40 °C, at an input power of 60 W, the maximum steady-state evaporator temperature for the FMHP is nearly 100 °C, while for the copper plate the maximum evaporator temperature is 160°C. This results in a decrease in temperature gradients of approximately 60 °C. The heat source-heat sink temperature difference, $\Delta T = T_{ev} - T_c$, for T_{sf} = 40 °C when the FMHP is oriented horizontally, are plotted as a function of the applied heat flux rate in Fig. 9. Also shown for comparison is the heat source-heat sink temperature difference for a copper plate. The maximum evaporator temperature and temperature gradients for the FMHP are considerably smaller than those obtained for the copper plate. As shown in Fig. 9, the heat pipe operation reduces the slope of the temperature profile for the FMHP. This gives some indication of the ability of such FMHP to reduce the thermal gradients or localized hot spots. The size of the source-sink temperature difference for the FMHP increases in direct proportion of the input heat flux rate and varies from almost 10 °C at low power levels to approximately 50 °C at input power levels of approximately 60 W. This plot again shows the effectiveness of the enhanced FMHP and clearly indicates the temperature reduction level that can be expected at higher heat flux rates prior to dry-out.

The effective end cap to end cap thermal resistance of the FMHP is given in Fig. 10. Effective end cap to end cap thermal resistance, R_{tht}, defined here as the overall en cap to end cap temperature drop divided by the total applied heat load, Q. A common characteristic of the thermal resistance presented here is that the thermal resistance of the FMHP is high at low heat loads as a relatively thick liquid film resides in the evaporator. However, this thermal resistance decreases rapidly to its minimum value as the applied heat load is increased. This minimum value corresponds to the capillary limit. When the applied heat flux rate becomes higher than the capillary limit, the FMHP thermal resistance increases since the evaporator becomes starved of liquid. This is due to the fact that the capillary pumping cannot overcome the pressure losses within the FMHP. The decrease of the FMHP thermal resistance is attributed mainly to the decrease of the evaporator thermal resistance when the heat flux increases. Indeed, increasing the heat flux leads to the enhancement evaporation process in the grooves. The decrease of R_{tht} is observed when the evaporation process is dominated by the capillary limit. However, for heat fluxes higher than the maximum capillary limit, intensified boiling process may occur in the capillary structure, and consequently the evaporator thermal resistance increases. This results in an increase of the overall FMHP thermal resistance.

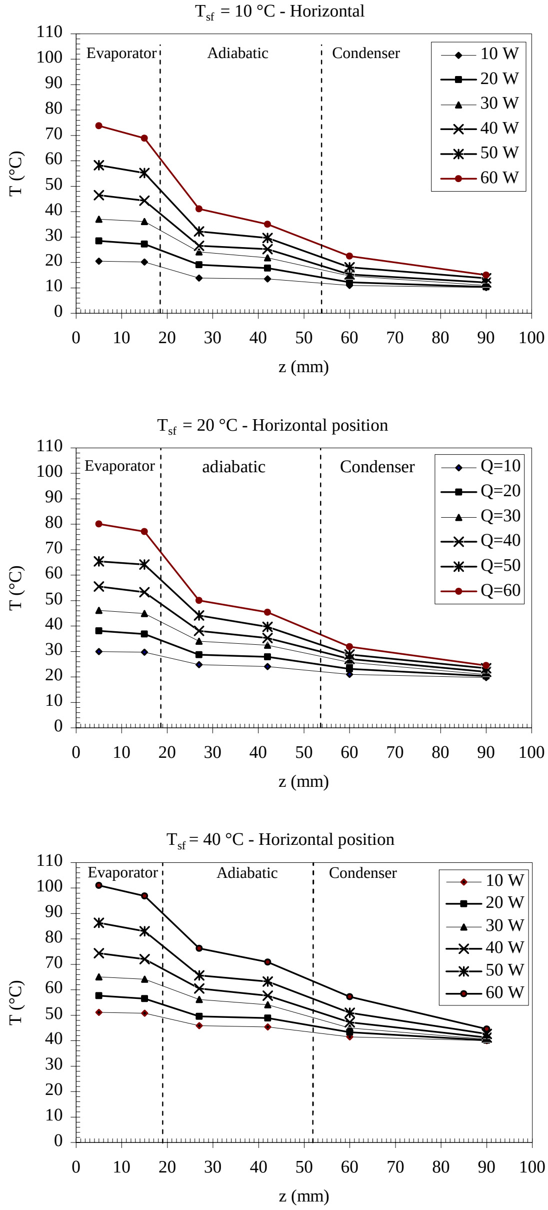

Fig. 7. FMHP axial temperature profile obtained for different heat sink temperatures (Horizontal position)

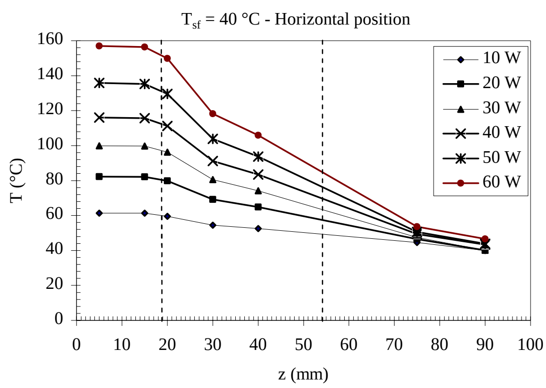

Fig. 8. Copper plate axial temperature profile

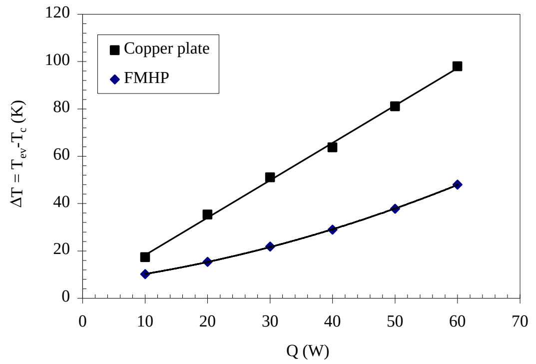

Fig. 9. Evaporator-Condenser temperature difference variations Vs. Q (Horizontal position, T_{sf} = 40 °C)

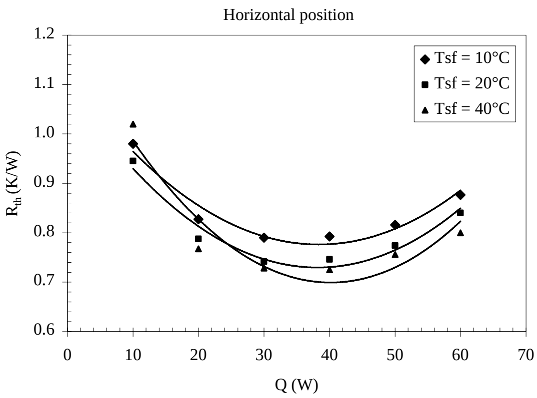

Fig. 10. FMHP thermal resistance Vs. Q, for different heat sink temperatures (Horizontal position)

It is also noticed that for a given heat flux rate the thermal resistance decreases as the heat sink temperature increases and the capillary limit, Q_{max}, increases. The increase in Q_{max} with T_{sf} is due to the decrease of the overall pressure drop ($\Delta P_l + \Delta P_v$). Indeed, when T_{sf} increases, the vapor temperature, T_{sat}, increases too. This results in a dramatic decrease of the vapor friction factor and consequently the vapor pressure drop ΔP_v decreases. However, the liquid pressure drop, ΔP_l increases with T_{sf} because an augmentation of the liquid mass flow rate is allowed by a decrease of the liquid friction factor with T_{sf}. Since the increase in ΔP_l is lower than the decrease in ΔP_v, the overall pressure drop ($\Delta P_l + \Delta P_v$) decrease. As shown in Fig. 10, the effect the heat sink temperature on the FMHP thermal resistance is effective when the heat input power is greater than the capillary limit.

In order to quantify the experimental results better, additional data are taken from which an effective FMHP conductivity, λ_{eff}, could be calculated using Fourier's law. The axial heat flux rate, that is, the heat transported through the FMHP in the direction of the grooves, is computed by dividing the input power by the FMHP cross-sectional area. This value is then divided by the source-sink temperature difference. The obtained result is then multiplied by the linear distance between the points at which the source and sink temperatures are measured. As depicted in Fig. 11, the increasing trend observed in the effective thermal conductivity of the FMHP results from the decreasing temperature gradient occurring at high heat flux rates which makes the heat pipes perform more effectively.

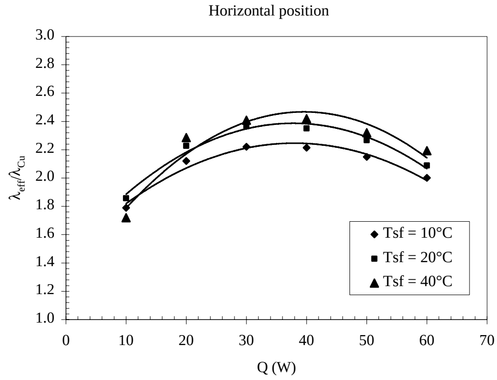

Fig. 11. Effective thermal conductivity enhancement variations Vs. Q, for different heat sink temperatures (Horizontal position)

The heat transfer coefficients in the evaporator and condenser zones are calculated according to the following expressions

$$h_{ev} = \frac{1}{\frac{(T_{ev} - T_{sat})}{q_{ev}} - \frac{t_w}{\lambda_w}} \tag{9}$$

$$h_c = \frac{1}{\frac{(T_{sat} - T_c)}{q_c} - \frac{t_w}{\lambda_w}} \tag{10}$$

q_{ev} and q_c are the heat fluxes calculated on the basis the evaporator and condenser heat transfer areas. t_w and λ_w are the thickness and the thermal conductivity of the wall, respectively.

The variations of the evaporation and condensation heat transfer as a function of the heat input power are depicted in Fig. 12, for different heat sink temperatures. The evaporation heat transfer coefficients are larger than the condensation ones. For a given heat sink temperature, the evaporation heat transfer coefficient exhibits a maximum which corresponds to the capillary limit, Q_{max}. The degradation of the evaporation process is caused by the fact that, for heat input powers which are higher than the capillary limit, the evaporator becomes starved of liquid and dry-out occurs since the capillary pumping is not sufficient for these conditions to overcome the liquid and vapor pressure losses. The condensation heat transfer coefficient increases with the heat input power, Q. This is due to the fact that the FMHP is correctly filled, and the blocking zone at the end of the condenser section is not large. For a given heat input power, the evaporation heat transfer coefficient increases with the heat sink temperature, however, the condensation heat transfer coefficient seems to decrease when the heat sink temperature increases. Hence, the evaporation process in the grooves is enhanced when the heat sink temperature increases; meanwhile the condensation process is altered.

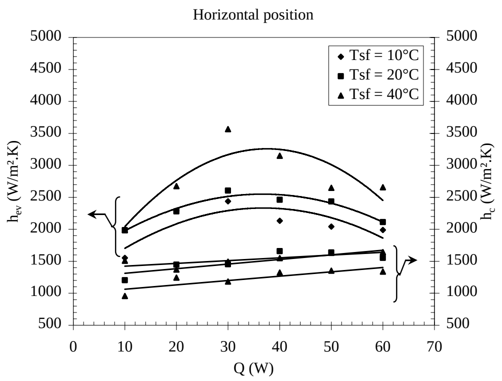

Fig. 12. Evaporation and condensation heat transfer coefficients Vs. Q, for different heat sink temperatures (Horizontal position)

B. Combined Effects of the Heat Input Power and the Tilt Angle

To determine the significance of the gravitational forces, experiments are carried out with different FMHP orientations: horizontal, thermosyphon, and anti-gravity positions. The heat sink temperature is fixed at T_{sf} = 40°C. The FMHP thermal resistances variations as a function of the heat input power are depicted in Fig. 13, for different FMHP orientations. For heat flux rates Q > 40 W, the FMHP thermal resistances are nearly the same for the different positions (if we consider the uncertainties on thermal resistance). However, for heat flux rates Q < 40 W, the FMHP becomes sensitive to the orientation. The Anti-gravity position exhibits the highest thermal resistances, while the thermosyphon and the horizontal positions exhibit similar thermal resistances which are lower than those obtained for the anti-gravity position.

In Fig. 14 are depicted the variations of the ratio of the effective thermal conductivity, λ_{eff}, to the copper thermal conductivity, λ_{eff} , as a function of the heat power input. The enhancement of the effective thermal conductivity of the FMHP amounts to an increase of nearly 240 percent for an input heat flux rate of about 40 W, for the horizontal and thermosyphon positions, however, for the anti-gravity position, the enhancement is lower and varies from nearly 30% for a heat input power of 10 W to 220% for a heat input power of 40 W, and decreases to 200% for Q = 60 W.

Fig. 15 shows the variations of the evaporator and condensation heat transfer coefficients as a function of the heat input power, Q. As it can be noticed, the evaporator heat transfer coefficients are not very sensitive to the FMHP orientation (if we consider the uncertainties). We can also notice that for heat input powers, which are higher than the capillary limit, the evaporator heat transfer coefficients are higher than those obtained for the horizontal and anti-gravity positions. However, the condensation heat transfer coefficient is sensitive to the orientation. These results can be explained by the liquid distribution inside the FMHP which is dependent on its orientation since the thermosyphon position is favorable to the return of the liquid to the evaporator.

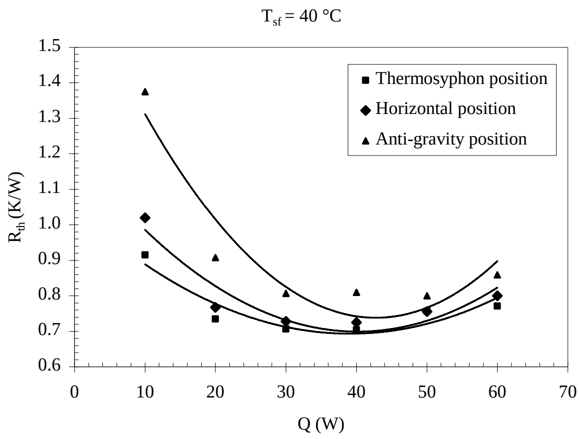

Fig. 13. FMHP thermal resistance Vs. Q, for different orientations

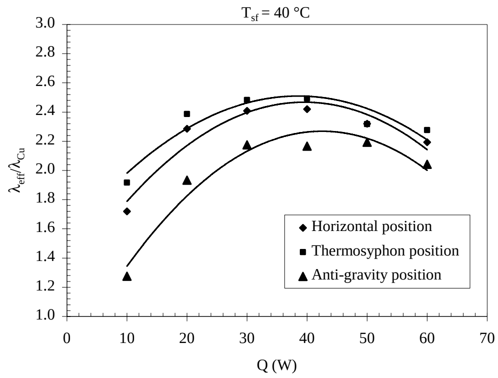

Fig. 14. Effective thermal conductivity enhancement variations as a function of Q, for different orientations (T_{sf} = 40 °C)

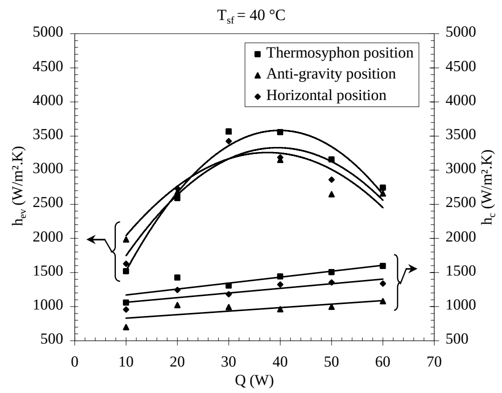

Fig. 15. Evaporation and condensation heat transfer coefficient Vs. Q, for different orientations (T_{sf} = 40 °C)

C. Heat Transfer Law

In order to quantify the heat transfer mechanisms in the evaporator and condenser zones, we have processed the experimental data in dimensionless numbers in order to obtain heat transfer laws. The dimensionless analysis is carried out on the basis of Vaschy-Backingham theorem (or π theorem). The heat transfer coefficients in the evaporator and condenser zones are calculated according to (9) and (10).The following dimensionless numbers are evidenced from the π analysis:

(i) the Laplace constant (obtained for Bond number equal to unity), La

$$La = \sqrt{\frac{\sigma}{(\rho_l - \rho_v)g}} \tag{11}$$

where σ is the liquid surface tension. ρ_l and ρ_v are the liquid and vapor densities, respectively. g is the gravity acceleration.
(ii) the Reynolds number, Re

$$Re = \frac{\rho_l V_e La}{\mu_l} = \frac{\dot{m}}{\mu_l S} = \frac{Q}{\mu_l S \ \Delta h_v} = \frac{q}{\mu_l \ \Delta h_v} \tag{12}$$

where V_e is the liquid or the vapor velocity. μ_l is the liquid dynamic viscosity, and Δh_v is the latent heat. S is the heat transfer area in the evaporator ($l_e \times L_e$) or condenser section ($l_c \times L_c$), Q is the heat flux rate, and q is the heat flux transferred in the evaporator or the condenser zone.
(iii) the Prandtl number, Pr

$$Pr = \frac{\mu_l C_{pl}}{\lambda_l} \tag{13}$$

where C_{pl} is the liquid specific heat, and λ_l is the liquid thermal conductivity.
(iv) the Nusselt number, Nu

$$Nu = \frac{h \ La}{\lambda_l} \tag{14}$$

where h is the heat transfer coefficient in the evaporator or condenser section.
(v) the modified Jakob number, Ja*

$$Ja^* = \frac{\rho_l}{\rho_v} \frac{C_{pl} \ T_{sat}}{\Delta h_v} \tag{15}$$

Hence, the heat transfer coefficients can be calculated by

$$Nu = A \, Re^{m_1} \ Pr^{m_2} \ Ja^{*m_3} \tag{16}$$

A, m_1, m_2, and m_3 are constants, which are determined from the experimental results. For the evaporation heat transfer, relation (16) is calculated by taking the liquid physical properties at the saturation temperature and the vapor physical properties at the film temperature (T_f = (T_{sat}+T_w)/2). For condensation heat transfer, the liquid and vapor physical properties are determined by considering the film and saturation temperatures, respectively.

The constants of (16) are determined from the experimental data by a linear regression analysis, for the evaporation and the condensation phenomena. It is found that the heat transfer law proposed by (16), the experimental results are well correlated when considering A = 902, m_1 = 0.825, m_2 = 0.333, m_3 = -0.999, and m_4 = -0.020, for the evaporation phenomenon, and A = 2.165×10^{-12}, m_1 = 1.001, m_2 = -0.032, m_3 = 2.644, and m_4 = 1.907, for the condensation phenomenon. The variations of the calculated Nusselt number as a function of the Nusselt number obtained experimentally are depicted in Figs. 16 and 17. As it can be seen from Fig. 16, the experimental Nusselt number for the heat transfer by evaporation is well represented by equation (16). For the evaporation heat transfer, the coefficient of correlation is 0.751 and the deviation from the experimental results is ± 20%. For the condensation heat transfer law, the experimental results are very well represented by equation (16) with a coefficient of correlation of 0.978, and the deviation from the experimental results is ± 10%.

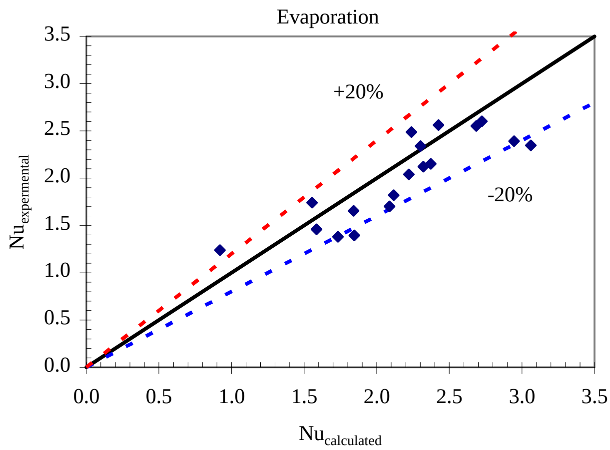

Fig. 16. Comparison between the Nusselt number obtained from the experimental results and that obtained from (16) for the evaporation heat transfer

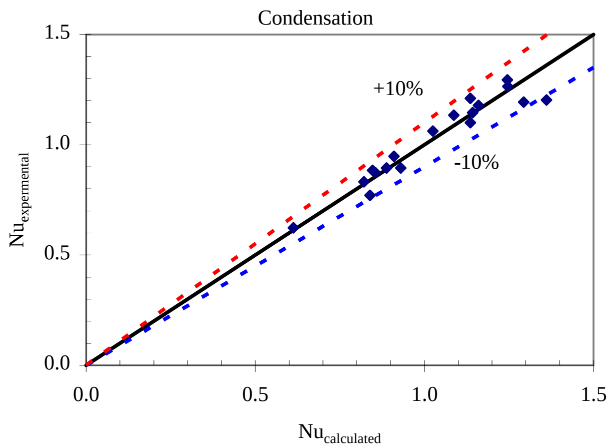

Fig. 17. Comparison between the Nusselt number obtained from the experimental results and that obtained from (16) for the condensation heat transfer

VI. FMHP Modeling

The section of the FMHP is illustrated by Fig. 3 (square microchannels with D_g = W_g = d). The liquid accumulates in the corners and forms four meniscuses (Fig. 18). Their curvature radius, r_c, is related to the difference of pressure, between vapor and liquid phase, by the Laplace-Young equation.

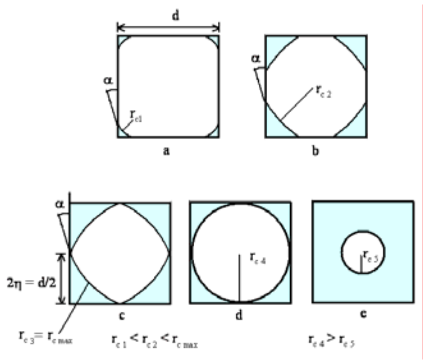

Fig. 18. Evolution of the curvature radius of the liquid-vapor interface along a microchannel

In the evaporator and adiabatic zones, the curvature radius, in the parallel direction of the microchannel axis, is lower than the one perpendicular to this axis. Therefore, the meniscus is described by only one curvature radius. In a given section, r_c is supposed constant. The axial evolution of r_c is obtained by the differential of the Laplace-Young equation. The part of wall that is not in contact with the liquid is supposed dry and adiabatic.

In the condenser, the liquid flows toward the microchannel corners. There is a transverse pressure gradient, and a transverse curvature radius variation of the meniscus. The distribution of the liquid along a microchannel is presented in Fig. 18.

The microchannel is divided into several elementary volumes of length, dz, for which, we consider the Laplace-Young equation, and the conservation equations written for the liquid and vapor phases as it follows:

Laplace-Young equation

$$\frac{dP_v}{dz}-\frac{dP_l}{dz}=-\frac{\sigma}{r_c^2}\frac{dr_c}{dz} \tag{17}$$

Liquid and vapor mass conservation

$$\frac{d\left(\rho_l\ w_l\ A_l\right)}{dz}=\frac{1}{\Delta h_v}\frac{dQ}{dz} \tag{18}$$

$$\frac{d\left(\rho_v\ w_v\ A_v\right)}{dz}=-\frac{1}{\Delta h_v}\frac{dQ}{dz} \tag{19}$$

Liquid and vapor momentum conservation

$$\rho_l\frac{d(\ A_l w_l^2\ )}{dz}dz= \frac{d(\ A_l P_l\ )}{dz}dz+A_{il}\left|\tau_{il}\right|+A_{lw}\left|\tau_{lw}\right|-\ \rho_l\ g\ A_l\ sin\,\beta\ dz \tag{20}$$

$$\rho_v\frac{d(\ A_v w_v^2\ )}{dz}dz\ = -\frac{d(\ A_v\ P_v\ )}{dz}dz-\left|\tau_{il}\right|A_{il}-\left|\tau_{vw}\right|A_{vw}-\rho_v\ g\ A_v\ sin\,\beta\ dz \tag{21}$$

Energy conservation

$$\lambda_w\frac{\partial^2 T_w}{\partial z^2}-\frac{h}{t_w}\left(T_w-T_{sat}\right)=-\frac{1}{l\times t_w}\frac{dQ}{dz} \tag{22}$$

The quantity dQ/dz in (18), (19), and (22) represents the heat flux rate variations along the elementary volume in the evaporator and condenser zones, which affect the variations of the liquid and vapor mass flow rates as it is indicated by (18) and (19). So, if the axial heat flux rate distribution along the microchannel is given by

$$Q=\begin{cases} Q_a\ z/L_e & 0\le z\le L_e \\ Q_a & L_e<z\ <L_e+L_a \\ Q_a\left(1+\dfrac{L_e+L_a\text{ - }z}{L_c\text{ - }L_b}\right) & L_e+L_a\le z\le L_t-L_b \end{cases} \tag{23}$$

we get a linear flow mass rate variations along the microchannel.

In equation (23), h represents the heat transfer coefficient in the evaporator, adiabatic and condenser sections. For these zones, the heat transfer coefficients are determined from the experimental results (section IV.C). Since the heat transfer in the adiabatic section is equal to zero and the temperature distribution must be represented by a mathematical continuous function between the different zones, the adiabatic heat transfer coefficient value is equal to infinity.

The liquid and vapor passage sections, A_l, and A_v, the interfacial area, A_{il}, the contact areas of the phases with the wall, A_{lp} and A_{vp}, are expressed using the contact angle and the interface curvature radius by

$$A_l=4*r_c{}^2\left(sin^2\theta-\theta+\frac{sin\,2\theta}{2}\right) \tag{24}$$

$$A_v=d^2-A_l \tag{25}$$

$$A_{il}=8\times\theta\times r_c\times dz \tag{26}$$

$$\mathrm{A}_{\mathrm{lw}}=\frac{16}{\sqrt{2}}\mathrm{r_c}\sin\theta\ \mathrm{dz} \tag{27}$$

$$A_{vw}=\left(4\times d\text{ - }\frac{16}{\sqrt{2}}r_c\ sin\,\theta\ \right)dz \tag{28}$$

$$\theta=\frac{\pi}{4}-\alpha \tag{29}$$

The liquid-wall and the vapor-wall shear stresses are expressed as

$$\tau_{lw}=\frac{1}{2}\rho_l w_l^2 f_l\ ,\ \ f_l=\frac{k_l}{R_{e_l}};\ R_{el}=\frac{\rho_l w_l D_{hlw}}{\mu_l} \tag{30}$$

$$\tau_{vw}=\frac{1}{2}\rho_v w_v^2 f_v\ ,\ f_v=\frac{k_v}{R_{ev}}\ ,\ R_{ev}=\frac{\rho_v w_v D_{hvw}}{\mu_v} \tag{31}$$

Where k_l and k_v are the Poiseuille numbers, and D_{hlw} and D_{hvw} are the liquid-wall and the vapor-wall hydraulic diameters, respectively.

The hydraulic diameters and the shear stresses in equations (30) and (31) are expressed as follows

$$D_{hlw} = \frac{\sqrt{2} \times r_c \left(sin^2 \theta - \theta + \frac{sin 2\theta}{2} \right)}{sin \theta} \qquad (32)$$

$$D_{hvw} = \frac{d^2 - 4 r_c^2 \left(sin^2 \theta - \theta + \frac{sin 2\theta}{2} \right)}{d - \frac{4}{\sqrt{2}} sin\theta \times r_c} \qquad (33)$$

$$\tau_{lw} = \frac{1}{2} \frac{k_l w_l \mu_l \, sin\theta}{2\sqrt{2} \left(sin^2 \theta - \theta + \frac{sin\theta}{2} \right) r_c} \qquad (34)$$

$$\tau_{vw} = \frac{k_v w_v \mu_v \left(d - \left(\frac{4}{\sqrt{2}} sin\theta \right) r_c \right)}{2 \left(d^2 - 4 r_c^2 \left(sin^2 \theta - \theta + \frac{sin\theta}{2} \right) \right)} \qquad (35)$$

The liquid-vapor shear stress is calculated by assuming that the liquid is immobile since its velocity is considered to be negligible when compared to the vapor velocity ($w_l << w_v$). Hence, we have

$$\tau_{il} = \frac{1}{2} \frac{\rho_v w_v^2 k_v}{R_{eiv}} \quad R_{eiv} = \frac{\rho_v |w_v| D_{hiv}}{\mu_v} \qquad (36)$$

where D_{hiv} is the hydraulic diameter of the liquid-vapor interface. The expressions of D_{hiv} and τ_{iv} are

$$D_{hi} = \frac{d^2 - 4 r_c^2 \left(sin^2 \theta - \theta + \frac{sin 2\theta}{2} \right)}{2 \ \theta \ r_c} \qquad (37)$$

$$\tau_{il} = \frac{k_v \theta \ r_c w_v \mu_v}{d^2 - 4 r_c^2 \left(sin^2 \theta - \theta + \frac{sin 2\theta}{2} \right)} \qquad (38)$$

The equations (17-22) constitute a system of six first order differential, nonlinear, and coupled equations. The six unknown parameters are: r_c, w_l, w_v, P_l, P_v, and T_w. The integration starts in the beginning of the evaporator (z = 0) and ends in the condenser extremity ($z = L_t - L_b$), where L_b is the length of the condenser flooding zone. The boundary conditions for the adiabatic zone are the calculated solutions for the evaporator end. In z = 0, we use the following boundary conditions:

$$\begin{cases} r_c|^0 = r_{cmin} & (a) \\ w_l|^0 = w_v|^0 = 0 & (b) \\ P_v|^0 = P_{sat}(T_v) & (c) \\ P_l|^0 = P_v - \frac{\sigma}{r_{cmin}} & (d) \end{cases} \qquad (39)$$

The solution is performed along the microchannel if r_c is higher than r_{cmin}. The coordinate for which this condition is verified, is noted L_{as} and corresponds to the microchannel dry zone length. Beyond this zone, the liquid doesn't flow anymore. Solution is stopped when $r_c = r_{cmax}$, which is determined using the following reasoning: the liquid film meets the wall with a constant contact angle. Thus, the curvature radius increases as we progress toward the condenser (Figs. 18a to 18b). When the liquid film contact points meet, the wall is not anymore in direct contact with vapor. In this case, the liquid configuration should correspond to Fig. 18c, but actually, the continuity in the liquid-vapor interface shape imposes the profile represented on Fig. 15d. In this case, the curvature radius is maximum. Then, in the condenser, the meniscus curvature radius decreases as the liquid thickness increases (Fig. 18e). The transferred maximum power, so called capillary limit, is determined if the junction of the four meniscuses starts precisely in the beginning of the condenser.

VII. Numerical Results and Analysis

In this analysis, we study a FMHP with the dimensions which are indicated in Table 4. The capillary structure is composed of microchannels as it is represented by the sketch of Fig. 3. The working fluid is water and the heat sink temperature is equal to 40 °C. The conditions of simulation are such as the dissipated power is varied, and the introduced mass of water is equal to the optimal fill charge.

The variations of the curvature radius r_c are represented in Fig. 19. In the evaporator, because of the recession of the meniscus in the channel corners and the great difference of pressure between the two phases, the interfacial curvature radius is very small on the evaporator extremity. It is also noticed that the interfacial curvature radius decreases in the evaporator section when the heat flux rate increases. However, it increases in the condenser section. Indeed, when the heat input power increases, the liquid and vapor pressure losses increase, and the capillary pressure become insufficient to overcome the pressure losses. Hence, the evaporator becomes starved of liquid, and the condenser is blocked with the liquid in excess.

The evolution of the liquid and vapor pressures along the microchannel is given in Figs. 20 and 21. We note that the vapor pressure gradient along the microchannel is weak. It is due to the size and the shape of the microchannel that don't generate a very important vapor pressure drop. For the liquid, the velocity increase is important near of the evaporator extremity, which generates an important liquid pressure drop.

Figure 22 presents the evolution of the liquid phase velocity along a microchannel. In the evaporator section, as the liquid passage section decreases, the liquid velocity increases considerably. On other hand, since the liquid passage section increases along the microchannel (adiabatic and condenser sections), the liquid velocity decreases to reach zero at the final extremity of the condenser. In the evaporator, the vapor phase velocity increases since the vapor passage section decreases. In the adiabatic zone, it continues to grow with the reduction of the section of vapor passage. Then, when the condensation appears, it decreases, and it is equal to zero on the extremity of the condenser (Fig. 23).

The variations of the wall temperature along the FMHP are reported in Fig. 24. In the evaporator section, the wall temperature decreases since an intensive evaporation appears due the presence of a thin liquid film in the corners. In the adiabatic section, the wall temperature is equal to the saturation temperature corresponding to the vapor pressure. In the condenser section, the wall temperature decreases. In this plot, are shown a comparison between the numerical results and the experimental ones, and a good agreement is found between the temperature distribution along the FMHP computed from the model and the temperature profile which is measured experimentally. An agreement is also noticed between the temperature distribution which is obtained from a pure conduction model and that obtained experimentally (Fig. 25).

VIII. Conclusion

In this study, a copper FMHP is machined, sealed and filled with water as working fluid. The temperature measurements allow for a determination of the temperature gradients and maximum localized temperatures for the FMHPs. The thermal FMHP are compared to those of a copper plate having the same dimensions. In this way, the magnitude of the thermal enhancement resulting from the FMHPs could be determined. The thermal measurements show significantly reduced temperature gradients and maximum temperature decrease when compared to those of a copper plate having the same dimensions. Reductions in the source-sink temperature difference are significant and increases in the effective thermal conductivity of approximately 250 percent are measured when the FMHPs operate horizontally.

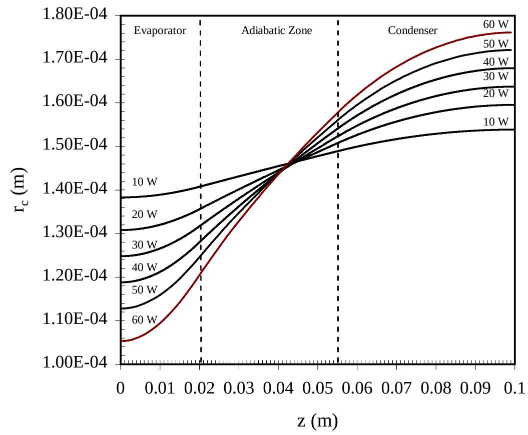

Fig. 19. Variations of the curvature radius r_c of the meniscus

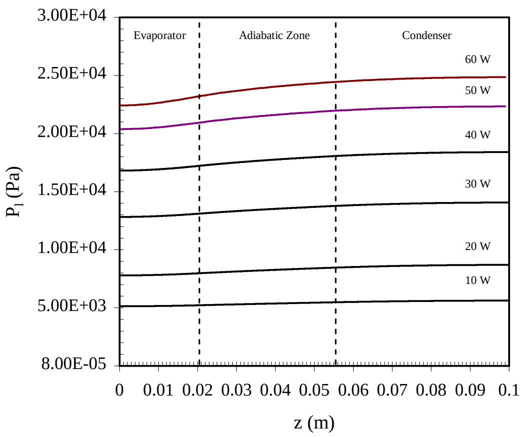

Fig. 21. Variations of the liquid pressure P_l

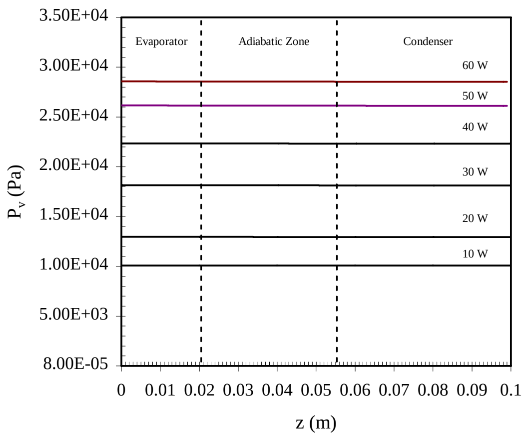

Fig. 20. Variations of the vapor pressure P_v

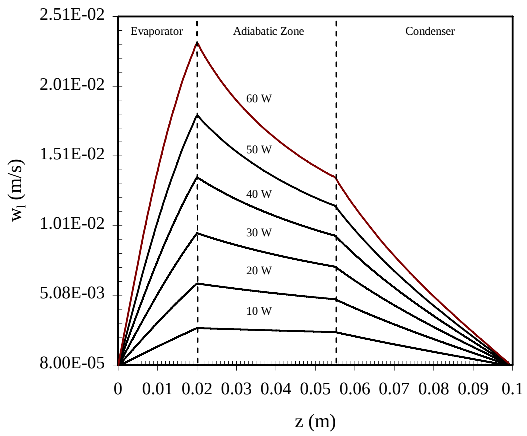

Fig. 22. The liquid phase velocity distribution

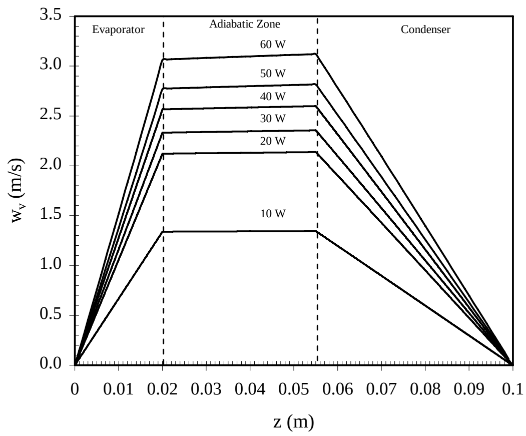

Fig. 23. The liquid phase velocity distribution

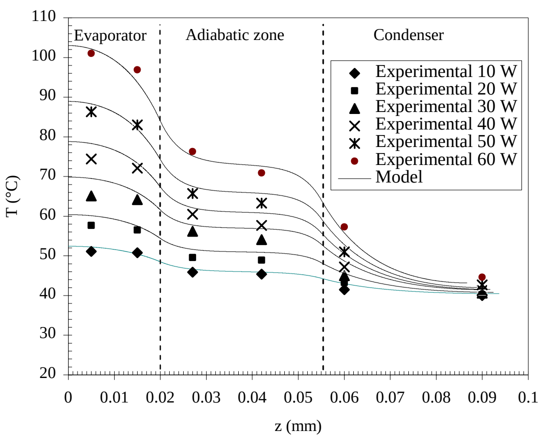

Fig. 24. Variations of the FMHP wall temperature

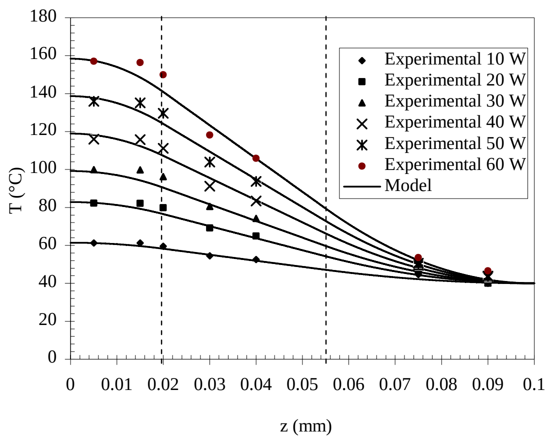

Fig. 25. Variations of the copper plate wall temperature

The main feature of this study is the establishment of heat transfer laws for both condensation and evaporation phenomena. Appropriate dimensionless numbers are introduced and allow for the determination of relations, which represent well the experimental results. This kind of relations will be useful for the establishment of theoretical models for such capillary structures.

Based on the mass conservation, momentum conservation, energy conservation, and Laplace-Young equations, a one dimensional numerical model is developed to simulate the liquid-vapor flow as well as the heat transfer in a FMHP constituted by microchannels. It allows to predict the maximum power and the optimal mass of the fluid. The model takes into account interfacial effects, the interfacial radius of curvature, and the heat transfer in both the evaporator and condenser zones. The resulting coupled ordinary differential equations are solved numerically to yield interfacial radius of curvature, pressure, velocity, temperature information as a function of axial distance along the FMHP, for different heat inputs. The model results predict an almost linear profile in the interfacial radius of curvature. The pressure drop in the liquid is also found to be about an order of magnitude larger than that of the vapor. The model predicts very well the temperature distribution along the FMHP.

Although not addressing several issues such as the effect of the fill charge, FMHP orientation, heat sink temperature, and the geometrical parameters (groove width, groove height or groove spacing), it is clear from these results that incorporating such FMHP as part of high integrated electronic packages can significantly improve the performance and reliability of electronic devices, by increasing the effective thermal conductivity, decreasing the temperature gradients and reducing the intensity and the number of localized hot spots.

REFERENCES

[1] M. Groll, M. Schneider, V. Sartre, M.C. Zaghdoudi, and M. Lallemand, “Thermal Control of electronic equipment by heat pipes,” *Revue Générale de Thermique*, vol. 37, no. 5, 1998, pp. 323-352.

[2] T.P. Cotter, “Principles and Prospects of Micro Heat Pipes,” *5th International Heat Pipe Conference*, Tsukuba, Japan, May 14-18, 1984, pp. 328-335.

[3] A. Itoh, and F. Polasek, “Development and Application of Micro Heat pipes,” *7th International Heat Pipe Conference*, Minsk, Russia, May 21-25, 1990.

[4] Z. Ji, W. Caiyou, Y. Xiuqin, and Z. Zeqing, “Experimental Investigation of the Heat Transfer Characteristics of the Micro Heat Pipes,” *8th International Heat Pipe Conference*, Bejing, China, September 14-18, 1992, pp. 416-420.

[5] B.R. Babin, G.P. Peterson, and D. Wu, “Analysis and Testing of a Micro Heat Pipe During Steady-State,” *ASME/AIchE National Heat*

Transfer Conference, Paper No. 89-HT-17, Philadelphia, Pennsyvania, USA, August 5-8, 1989, 10p.

[6] B.R. Babin, G.P. Peterson, and D. Wu, "Steady-State Modeling and Testing of Micro Heat Pipe," *Journal of Heat Transfer*, vol. 112, 1990, pp. 595-601.

[7] D. Wu, and G.P. Peterson, "Investigation of the Transient Characteristics of a Micro Heat Pipe," *Journal of Thermophysics and Heat Transfer*, vol. 5, no. 2, 1991, pp. 129-134.

[8] D. Wu, G.P. Peterson, and W.S. Chang, "Transient Experimental Investigation of Micro Heat pipes," *Journal of Thermophysics and Heat Transfer*, vol. 5, no. 4, 1991, pp. 539-545.

[9] S.H. Moon, C.J. Kim, B.H. Kim, S.E. Hong, and J.S. Lee, "An Experimental Study on the Performance Limitation of a Micro Heat Pipe with Triangular Cross-Section," *10th International Heat Pipe Conference*, Tokyo, Japan, September 22-26, 1999, pp. 15-19.

[10] G.P. Peterson, "Heat Pipes in the Thermal Control of Electronic Components," *3rd International Heat Pipe Symposium*, September 12-14, Tsukuba, Japan, 1988, pp. 2-12.

[11] G.P. Peterson, A.B. Duncan, A.S. Ahmed, A.K. Mallik, and M.H. Weichold, "Experimental Investigation of Micro Heat Pipes in Silicon Wafers," *Micromechanical Sensors, Actuators, and Systems*, DSC-Vol. 32, 1991, pp. 341-348.

[12] F.M. Gerner, "Micro Heat Pipes," *AFSOR Final Report*, No.S-210-10MG-066, Wright-Patterson AFB, Dayton, OH, USA, 1990.

[13] A.K. Mallik, and G.P. Peterson, "On the Use of Micro Heat Pipes as an Integral Part of Semiconductors," *3rd ASME-JSME Thermal Engineering Joint Conference Proceeding*, vol. 2, Reno, NV, USA, March 17-22, 1991, pp. 394-401.

[14] F.M. Gerner, B. Badran, J.P. Longtin, P. Ramadas, T.H. Henderson, and W.S. Chang, "Flow and Heat Transfer Limitations in Micro Heat Pipes," *28th National Heat Transfer Conference*, August 9-12, San Diego, CA, USA, 1992, pp. 99-104.

[15] G.P. Peterson, A.B. Duncan, and M.H. Weichold, "Experimental Investigation of Micro Heat Pipes Fabricated in Silicon Wafers," *Journal of Heat Transfer*, vol. 115, 1993, pp. 751-756.

[16] F.M. Gerner, B. Badran, H.T. Henderson, and P. Ramadas, "Silicon-Water Micro Heat Pipes," *Thermal Science Engineering*, vol. 2, no.1, 1994, pp. 90-97.

[17] D. Shen, R. Mitchell, D. Dobranich, D. Adkins, and M. Tuck, "Micro Heat Spreader Enhanced Heat Transfer in MCMs," *IEEE Multi-Chip-Module Conference*, Santa Cruz, California, USA, January 31-February 2, 1995, pp. 189-194.

[18] D.A. Benson, D.R. Adkins, G.P. Peterson, R.T. Mitchell, M.R. Tuck, and D.W. Palmer, "Turning Silicon Substrates into Diamond: Micro Machining Heat Pipes," *Advances in Design, Materials and Processes for Thermal Spreaders and Heat Sinks Workshop*, Vail, CO, USA, April 19-21, 1996, pp. 19-21.

[19] D.A. Benson, D.R. Adkins, G.P. Peterson, R.T. Mitchell, M.R. Tuck, and D.W. Palmer, "Micro Machined Heat Pipes in Silicon MCM Substrates," *Proceeding of IEEE Multichip Module Conference*, Santa Cruz, CA, USA, November 6-7, 1996, pp. 127-129.

[20] D.A. Benson, R.T. Mitchell, M.R. Tuck, D.W. Palmer, and G.P. Peterson, "Ultrahigh-Capacity Micromachined Heat Spreaders," *Microscale Thermophysical Engineering*, vol. 2, no.1, 1998, pp. 21-30.

[21] B. Badran, F.M. Gerner, P. Ramadas, T. Henderson, and K.W. Baker, "Experimental Results for Low-temperature Silicon Micromachined Micro Heat Pipe Arrays Using Water and Methanol as Working Fluids," *Experimental Heat Transfer*, vol. 10, no. 4, 1997, pp. 253-272.

[22] B. Gromoll, "Micro cooling systems for high density packaging," *Revue Générale de la Thermique*, vol. 37, 1998, pp. 781-787.

[23] Y. Avenas, B. Mallet, C. Gillot, A. Bricard, C. Schaeffer, G. Poupon, and E. Fournier, "Thermal Spreaders for High Heat Flux Power Devices," *7th THERMINIC Workshop*, Paris, France, September 24-27, 2001, pp. 59-631.

[24] Y. Avenas, M. Ivanova, N. Popova, C. Schaeffer, J.L. Schanen, and A. Bricard, "Thermal Analysis of Thermal Spreaders Used in Power Electronics Cooling," *37th Annual Meeting of the Industry-Applications-Society, Conference Record of the 2002 IEEE Industry Applications Conference*, Pittsburgh, PA, USA, October 12-18, 2002, pp. 216-221.

[25] C. Gillot, Y. Avenas, N. Cezac, G. Poupon, C. Schaeffer, and E. Fournier, "Silicon Heat Pipes Used as Thermal Spreaders," *8th Intersociety Conference on Thermal and Thermomechanical Phenomena in Electronic Systems (ITHERM 2002)*, San Diego, USA, May 30- June 01, 2002, pp. 1052-1057.

[26] C. Gillot, Y. Avenas, N. Cezac, G. Poupon, C. Schaeffer, and E. Fournier, "Silicon Heat Pipes Used as Thermal Spreaders," *IEEE Transactions on Components and Packaging Technologies*, vol. 26, no. 2, 2003, pp. 332-339.

[27] C. Gillot, G. Poupon, Y. Avenas, C. Schaeffer, and E. Fournier, E., "Design and Fabrication of Flat Silicon Heat Pipes with Micro Capillary Grooves," *Houille Blanche-Revue Internationale de l'Eau*, no. 4, 2003, pp. 62-66.

[28] C. Gillot, A. Laï, M. Ivanova, Y. Avenas, C. Schaeffer, and E. Fournier, "Experimental Study of a Flat Silicon Heat Pipe with Microcapillary Grooves," *9th Intersociety Conference on Thermal and Thermomechanical Phenomena in Electronic Systems (ITHERM 2004)*, vol. 2, Las Vegas, NV, USA, June 1-4, 2004, pp. 47-51.

[29] M. Ivanova, C. Schaeffer, Y. Avenas, A. Laï, and C. Gillot, "Realization and Thermal Analysis of Silicon Thermal Spreaders used in power electronics cooling," *IEEE International Conference on Industrial Technology*, vol. 1-2, Maribor, Slovenia, December 10-12, 2003 pp. 1124-1129.

[30] M. Lee, M. Wong, and Y. Zohar, "Characterization of an Integrated Micro Heat pipe," *Journal of Micromechanics and Microengineering*, Vol.13, 2003, pp. 58-64.

[31] M. Lee, M. Wong, and Y. Zohar, "Integrated Micro Heat Pipe Fabrication Technology," *Journal of Microelectromechanical Systems*, vol. 12, no. 2, 2003, pp. 138-146.

[32] A. Laï, C. Gillot, M. Ivanova, Y. Avenas, C. Louis, C. Schaeffer, and E. Fournier, "Thermal Characterization of Flat Silicon Heat Pipes," *20th Annual IEEE Semiconductor Thermal Measurement and Management Symposium*, San Jose, CA, USA, 9-11 March, 2004, pp. 21-25.

[33] A.K. Mallik, G.P. Peterson, and W. Weichold, "Construction Processes for Vapor Deposited Micro Heat Pipes," *10th Symposium on Electronic Materials Processing and Characteristics*, Richardson, TX, USA, June 3-4, 1991.

[34] A.K. Mallik, G.P. Peterson, and M.H. Weichold, "On the Use of Micro Heat Pipes as an Integral Part of Semiconductor Devices," *Journal of Electronic Packaging*, vol. 114, 1992, pp. 436-442.

[35] M.H. Weichold, G.P. Peterson, and A. Mallik, "Vapor Deposited Micro Heat Pipes," *U.S. Patent 5,179,043*, 1993.

[36] G.P. Peterson, and A.K. Mallik, "Steady-State Investigation of Vapor Deposited Micro Heat Pipe Arrays," *Journal of Electronic Packaging*, vol. 117, no. 1, 1995, pp. 75-81.

[37] G.P. Peterson, and A.K. Mallik, "Transient Response of Vapor Deposited Micro Heat Pipe Arrays," *Journal of Electronic Packaging*, vol. 117, no. 1, 1995, pp. 82-87.

[38] D.R. Adkins, D.S. Shen, D.W. Palmer, and M.R. Tuck, "Silicon Heat Pipes for Cooling Electronics," *Proceeding of 1st Annual Spacecraft Thermal Control Symposium*, Albuquerque, NM, USA, November 16-18, 1994, 11p.

[39] M. Le Berre, S. Launay, V. Sartre, and M. Lallemand, "Fabrication and Experimental Investigation of Silicon Micro Heat Pipes for Cooling Electronics," *Journal of Micromechanics and Microengineering*, vol. 13, no. 3, 2003, pp. 436-441.

[40] S. Launay, M. Le Berre, V. Sartre, P. Morfouli, J. Boussey, D. Barbier, and M. Lallemand, "Fabrication of Silicon Micro Heat Pipes for Cooling Electronics," *Houille Blanche-Revue Internationale de l'Eau*, no. 4, 2003, pp. 82-87.

[41] S. Launay, V. Sartre, and M. Lallemand, "Experimental Study on Silicon Micro Heat Pipe Arrays," *Applied Thermal Engineering*, vol. 24, 2004, pp. 233-243.

[42] M. Le Berre, G. Pandraud, and P. Morfouli, "The performance of Micro Heat Pipes Measured by Integrated Sensors," *Journal of Micromechanical Microengineering*, vol. 16, no. 5, 2006, pp. 1047-1050.

[43] G. Pandraud, M. Le Berre, P. Morfouli, and M. Lallemand, "Influence of the fluid on the experimental performances of triangular silicon micro heat pipes," *Journal of Electronic Packaging*, vol. 128, no. 3, 2006, pp. 294-296.

[44] D.K. Harris, A. Palkar, G. Woncott, R. Dean, and F. Simionescu, "An Experimental Investigation in the Performance of Water-filled Silicon

Microheat Pipe Arrays," *Journal of Electronic Packaging*, vol. 132, no. 2, paper No.021005, 2010, 8p.

[45] S. Kalahasti, and Y. Joshi, "Performance Characterization of a Novel Flat Plate Micro Heat Pipe Spreader," *IEEE Transactions on Components and Packaging Technologies*, vol. 25, no. 4, 2002, pp. 554-560.

[46] S.W. Kang, S.H. Tsai, and H.C. Chen, "Fabrication and Test of Radial Grooved Micro Heat Pipes," *Applied Thermal Engineering*, vol. 22, no. 14, 2002, pp. 1559-1568.

[47] S.W. Kang, and D. Huang, "Fabrication of Star Grooves and Rhombus Grooves Micro Heat Pipe," *Journal of Micromechanics and Microengineering*, vol. 12, 2002, pp. 525-531.

[48] J.A. Kang, X. Fu, W.T. Liu, and P. Dario, "Investigation on Microheat Pipe Array with Arteries," *Journal of Thermophysics and Heat Transfer*, vol. 24, no. 4, 2010, pp. 803-810.

[49] C. Perret, Y. Avenas, Ch. Gillot, J. Boussey, and C. Schaeffer, "Integrated Cooling Devices in Silicon Technology," *The European Physical Journal Applied Physics*, vol. 18, no. 2, 2002, pp. 115-123

[50] M. Ivanova, A. Laï, C. Gillot, N. Sillon, C. Schaeffer, F. Lefèvre, M. Lallemand, and E. Fournier, "Design, Fabrication and Test of Silicon Heat Pipes With Radial Microcapillary Grooves," *10th Intersociety Conference on Thermal and Thermomechanical Phenomena in Electronic Systems (ITHERM 2006)*, vol. 1-2, San Diago, USA, 30 May – 2 June, 2006, pp. 545-551.

[51] S. Murthy, Y. Joshi & W. Nakayama, "Orientation Independent Two-phase Heat Spreaders for Space Constrained Applications," *Microelectronics Journal*, vol. 34, 2003, pp. 1187-1193.

[52] S. Murthy, Y. Joshi, and W. Nakayama, "Two-phase Heat Spreaders Utilizing Microfabricated Boiling Enhancement Structures," *Heat Transfer Engineering*, vol. 25, no. 1, 2004, pp. 25-36.

[53] R. Hopkins, A. Faghri, and D. Khrustalev, "Flat Miniature Heat Pipes with Micro Capillary Grooves," *Journal of Heat Transfer*, vol. 121, 1999, pp. 102-109.

[54] Y. Cao, M. Gao, J.E. Beam, and B. Donovan, "Experiments and Analyses of Flat Miniature Heat Pipes," *Journal of Thermophysics and Heat Transfer*, vol. 11, no. 2, 1997, pp. 158-164.

[55] Y. Cao, and M. Gao, "Wickless Network Heat Pipes for High Heat Flux Spreading Applications," *International Journal of Heat and Mass Transfer*, vol.45, 2002, pp. 2539-2547.

[56] L. Lin, R. Ponnappan, and J. Leland, "High Performance Miniature Heat Pipe," *International Journal of Heat and Mass Transfer*, vol. 45, 2002, pp. 3131-3142.

[57] M. Gao, and Y. Cao, "Flat and U-shaped Heat Spreaders for High-Power Electronics," *Heat Transfer Engineering*, vol. 24, 2003, pp. 57-65.

[58] J.C. Lin, J.C. Wu, C.T. Yeh, and C.Y. Yang, C.Y., "Fabrication and Performance Analysis of Metallic Micro Heat Spreader for CPU," *13th International Heat Pipe Conference*, Shangai, China, September 21-25, 2004, pp. 151-155.

[59] M.C. Zaghdoudi, C. Tantolin, C. Godet, "Experimental and Theoretical Analysis of Enhanced Flat Miniature Heat Pipes," *Journal of Thermophysics and Heat Transfer*, vol. 18, no. 4, 2004, pp. 430-447.

[60] F. Lefèvre, R. Rullière, G. Pandraud, and M. Lallemand, "Prediction of the Maximum Heat Transfer Capability of Two-Phase Heat Spreaders-Experimental Validation," *International Journal of Heat and Mass Transfer*, vol. 51, no. 15-16, 2008, pp. 4083-4094.

[61] S.H. Moon, G. Hwang, S.C. Ko, and Y.T. Kim, "Operating Performance of Micro Heat Pipe for Thin Electronic Packaging," *7th International Heat Pipe Symposium*, Jeju Island, South Korea, October 12-16, 2003, pp. 109-114.

[62] S.H. Moon, G. Hwang, S.C. Ko, & Y.T. Kim, "Experimental Study on the Thermal Performance of Micro-Heat Pipe with Cross-section of Polygon," *Microelectronics Reliability*, vol. 44, 2004, pp. 315-321.

[63] C. Romestant, G. Burban, and A. Alexandre, "Heat Pipe Application in Thermal-Engine Car Air Conditioning," *13th International Heat Pipe Conference*, Shanghai, China, September 21-25, 2004, pp. 196-201.

[64] W. Xiaowu, T. Yong, and C. Ping, "Investigation into Performance of a Heat Pipe with Micro Grooves Fabricated by Extrusion-Ploughing Process," *Energy Conversion and Management*, vol. 50, 2009, pp. 1384-1388.

[65] M. Schneider, M. Yoshida, and M. Groll, M., "Investigation of Interconnected Mini Heat Pipe Arrays For Micro Electronics Cooling," *11th International Heat Pipe conference*, Musachinoshi-Tokyo, Japan, September 12-16, 1999, 6p.

[66] M. Schneider, M. Yoshida, and M. Groll, "Optical Investigation of Mini Heat Pipe Arrays With Sharp Angled Triangular Grooves," *Advances in Electronic Packaging*, EEP-Vol. 26-1 and 26-2, 1999, pp. 1965-1969.

[67] M. Schneider, M. Yoshida, and M. Groll, "Cooling of Electronic Components By Mini Heat Pipe Arrays," *15th National Heat and Mass transfer Conference and 4th ISHMT/ASME Heat and Mass Transfer Conference*, Pune, India, January 12-14, 2000, 8p.

[68] H.T. Chien, D.S. Lee, P.P. Ding, S.L. Chiu, and P.H. Chen, "Disk-shaped Miniature Heat Pipe (DMHP) with Radiating Micro Grooves for a TO Can Laser Diode Package," *IEEE Transactions on Components and Packaging Technologies*, vol. 26, no. 3, 2003, pp. 569-574.

[69] H.Z. Tao, H. Zhang, J. Zhuang, and J.W. Bowmans, "Experimental Study of Partially Flattened Axial Grooved Heat Pipes," *Applied Thermal Engineering*, vol. 28, 2008, pp. 1699-1710.

[70] H.T. Lim, S.H. Kim, H.D. Im, K.H. Oh, and S.H. Jeong, "Fabrication and Evaluation of a Copper Flat Micro Heat Pipe Working under Adverse-Gravity Orientation," *Journal of Micromechanical Microengineering*, vol. 18, 2008, 8p.

[71] M. Murakami, T. Ogushi, Y. Sakurai, H. Masumuto, M. Furukawa, and R. Imai, "Heat Pipe Heat Sink," *6th International Heat Pipe Conference*, Grenoble, France, May 25-29, 1987, pp. 257-261.

[72] D. Plesh, W. Bier, and D. Seidel, "Miniature Heat Pipes for Heat Removal from Microelectronic Circuits," *Micromechanical Sensors, Actuators and Systems*, vol. 32, 1991, pp. 303-313.

[73] J.Y. Sun, and C.Y. Wang, "The Development of Flat Heat Pipes for Electronic Cooling," *4th International Heat Pipe Symposium*, Tsukuba, Japan, May 16-18, 1994, pp. 99-105.

[74] T. Ogushi, and G. Yamanaka, "Heat Transport Capability of Grooves Heat Pipes," *5th International Heat Pipe Conference*, pp. 74-79, Tsukuba, Japan, May 14-18, 1994, pp. 74-79.

[75] P. Soo Yong, and B. Joon Hong, "Thermal Performance of a Grooved Flat-Strip Heat Pipe with Multiple Source Locations," *7th International Heat Pipe Symposium*, Jeju Island, South Korea, October 12-16, 2003, pp. 157-162.

[76] L. Zhang, T. Ma, Z.F. Zhang, and X. Ge, "Experimental Investigation on Thermal Performance of Flat Miniature Heat Pipes with Axial Grooves," *13th International Heat Pipe Conference*, Shangai, China, September 21-25, 2004, pp. 206-210.

[77] N. Popova, C. Schaeffer, C. Sarno, S. Parbaud, and G. Kapelski, G., "Thermal management for stacked 3D microelectronic packages," *36th Annual IEEE Power Electronic Specialists Conference (PESC 2005)*, Recife, Brazil, June 12-16, 2005, pp. 1761-1766.

[78] N. Popova, C. Schaeffer, Y. Avenas, G. Kapelski, "Fabrication and Experimental Investigation of Innovative Sintered Very Thin Copper Heat Pipes for Electronics Applications, *37th IEEE Power Electronics Specialists Conference (PESC 2006)*, vol. 1-7, Cheju Island, South Korea, June 18-22, 2006, pp. 1652-1656.

[79] M. Zhang, Z. Liu, & G. Ma, "The experimental and numerical investigation of a grooved vapo chamber," *Applied Thermal Engineering*, vol. 29, 2009, pp. 422-430.

[80] M.C. Zaghdoudi, & C. Sarno, "Investigation on The Effects of Body Force Environment on Flat Heat Pipes," *Journal of Thermophysics and Heat Transfer*, vol. 15, no. 4, 2001, pp. 384-394.

[81] A. Faghri, *Heat pipe science and technology* (1st edition), Taylor & Francis, ISBN 1-56032-383-3, United States of America, 1995.

[82] G.P. Peterson, *An introduction to heat pipes - Modelling, testing and applications* (1st edition), John Wiley, United Stated of America, ISBM 0-471-30512-X, 1994.

[83] A.B. Duncan, and G.P. Peterson, "Charge Optimization for a Triangular-Shaped Etched Micro Heat Pipe," *Journal of Thermophysics*, vol. 9, no. 2, 1994, pp. 365-368.

[84] D. Khrustlev, A. Faghri, "Thermal Analysis of a Micro Heat Pipe," *Journal of Heat Transfer*, vol. 116, 1994, pp. 189-198.

[85] J.P. Longtin, B. Badran, and F.M. Gerner, "A one-dimensional model of a micro heat pipe during steady-state operation," *Journal of Heat Transfer*, vol. 116, 1994, pp. 709-715.

[86] G.P. Peterson, and H.B. Ma, "Theoretical Analysis of the Maximum Heat Transport in Triangular Grooves: a Study of Idealized Micro Heat Pipes, *Journal of Heat Transfer*, vol. 118, 1996, pp. 731-739.

[87] M.C. Zaghdoudi, V. Sartre, M. Lallemand, M., "Theoretical Investigation of Micro Heat Pipes," *10th International Heat Pipe Conference*, Stuttgart, Germany, September 22-26, 1997, 6p.

[88] J.M. Ha, and G.P. Peterson, "The Heat Transport Capacity of Micro Heat Pipes," *Journal of Heat Transfer*, vol. 120, 1998, pp. 1064-1071.

[89] H.B. Ma, & G.P. Peterson, G.P., "The Minimum Meniscus Radius and Capillary Heat Transport Limit in Micro Heat Pipes," *Journal of Heat Transfer*, vol. 120, 1998, pp. 227-233.

[90] C.B. Sobhan, H. Xiaoy Ang, and L.C. Yu, "Investigations on transient and steady-state performance of a micro heat pipe," *Journal of Thermophysics and Heat Transfer*, vol. 14, no. 1, 2000, pp. 161-169.

[91] K.H. Do, S.J. Kim, and J.K. Seo, "Mathematical Modeling and Thermal Optimization of a Micro Heat Pipe with Curved Triangular Grooves," *7th International Heat Pipe Symposium*, Jeju Island, South Korea, October 12-16, 2003, pp.325-331.

[92] B. Suman, S. De, and S. DasGupta, "A Model of the Capillary Limit of a Micro Heat Pipe and Prediction of the Dry-out Length," *International Journal of Heat and Fluid Flow*, vol. 26, 2005, pp. 495-505.

[93] B. Suman, and P. Kumar, "An Analytical Model for Fluid Flow and Heat Transfer in a Micro-Heat Pipe of Polygonal Shape," *International Journal of Heat and Mass Transfer*, Vol.48, 2005, pp. 4498-4509.

[94] Y.M. Hung, and Q. Seng, "Effects of Geometric Design on Thermal Performance of Star-groove Micro-Heat Pipes," *International Journal of Heat and Mass Transfer*, vol. 54, 2011, pp. 1198-1209.

[95] P.C. Wayner, Y.K. Kao, and L.V. Lacroix, "The Interline Heat Transfer Coefficient of an Evaporating Wetting Film," *International Journal of Heat and Mass Transfer*, vol.19, no.2, 1976, pp. 487-492.

[96] Y. Kamotani, Y., "Evaporator Film Coefficients of Grooved Heat Pipes," *3rd International Heat Pipe Conference*, Palo Alto, California, USA, September 22-24, 1978, 3p.

[97] F.W. Holm, and S.P. Goplen, "Heat Transfer in the Meniscus Thin Film Transition Region," *Journal of Heat Transfer*, vol. 101, 1979, pp. 543-547.

[98] P.C. Stephan, C.A. Büsse, "Analysis of the Heat Transfer Coefficient of Grooved Heat Pipe Evaporator Walls," *International Journal of Heat and Mass Transfer*, vol. 35, no. 2, 1992, pp. 383-391.

[99] L.W. Swanson, and G.P. Peterson, "Evaporating Extended Meniscus in a V-shaped Channel," *Journal of Thermophysics and Heat Transfer*, vol. 8, no. 1, 1994, pp. 172-180.

[100] D. Khrustlev, and A. Faghri, "Thermal Characteristics of Conventional and Flat Miniature Axially Grooved Heat Pipes," *Journal of Heat Transfer*, vol. 117, 1995, pp. 1048-1054.

[101] H.B. Ma, and G.P. Peterson, Temperature Variation and Heat Transfer in Triangular Grooves with an Evaporating Film, *Journal of Thermophysics and Heat Transfer*, vol. 11, no.1, 1997, pp. 90-97.

[102] A. Faghri, and D. Khrustalev, "Advances in modeling of enhanced flat miniature heat pipes with capillary grooves," *Journal of Enhanced Heat Transfer*, vol. 4, no. 2, 1997, pp. 99-109.

[103] D. Khrustlev, and A. Faghri, A., "Coupled Liquid and Vapor Flow in Miniature Passages with Micro Grooves," *Journal of Heat Transfer*, vol. 121, 1999, pp. 729-733.

[104] F. Lefèvre, R. Revellin, and M. Lallemand, "Theoretical Analysis of Two-Phase Heat Spreaders with Different Cross-section Micro Grooves," *7th International Heat Pipe Symposium*, Jeju Island, South Korea, October 12-16, 2003, pp. 97-102.

[105] S. Launay, V. Sartre, and M. Lallemand, "Hydrodynamic and Thermal Study of a Water-Filled Micro Heat Pipe Array," *Journal of Thermophysics and Heat Transfer*, vol. 18, no. 3, 2004, pp. 358-363.

[106] S. Tzanova, M. Ivanova, Y. Avenas, and C. Schaeffer, "Analytical Investigation of Flat Silicon Micro Heat Spreaders," *Industry Applications Conference, 39th IAS Annual Meeting Conference Record of the 2004 IEEE*, vol. 4, October 3-7, 2004, pp. 2296-2302.

[107] G. Angelov, S. Tzanova, Y. Avenas, M. Ivanova, T. Takov, C. Schaeffer, and L. Kamenova, "Modeling of Heat Spreaders for Cooling Power and Mobile Electronic Devices," *36th Power Electronics Specialists Conference (PESC 2005)*, Recife, Brazil, June 12-15, 2005, pp. 1080-1086.

[108] P.Z. Shi, K.M. Chua, S.C.K. Wong, and Y.M. Tan, "Design and Performance Optimization of Miniature Heat Pipe in LTCC," *Journal of Physics: Conference Series*, vol. 34, 2006, pp. 142-147.

[109] K.H. Do, S.J. Kim, and S.V. Garimella, "A Mathematical Model for Analyzing the Thermal Characteristics of a Flat Micro Heat Pipe with a Grooved Wick," *International Journal Heat and Mass Transfer*, vol.51, no.19-20, 2008, pp. 4637-4650.

[110] K.H. Do, and S.P. Jang, "Effect of Nanofluids on the Thermal Performance of a Flat Micro Heat Pipe with a Rectangular Grooved Wick," *International Journal of Heat and Mass Transfer*, vol.53, 2010, pp. 2183-2192.

[111] Y. Wang, and K. Vafai, "Transient Characterization of Flat Plate Heat Pipes During Startup and Shutdown operations," *International journal of Heat and Mass Transfer*, vol. 43, 2000, pp. 2641-2655.

[112] U. Vadakkan, J.Y. Murthy, S.V. Garimella, "Transport in Flat Heat Pipes at High Fluxes from Multiple Discrete Sources," *Journal of Heat Transfer*, vol. 126, 2004, pp. 347-354.

[113] L. Kamenova, Y. Avenas, S. Tzanova, N. Popova, and C. Schaeffer, "2D Numerical Modeling of the Thermal and Hydraulic Performances of a Very Thin Sintered Powder Copper Flat Heat pipe," *37th IEEE Power Electronics Specialist Conference (PESC 2006)*, Cheju Island, South Korea, June 18-22, 2006, pp. 1130-1136.

[114] F. Lefèvre, and M. Lallemand, "Coupled Thermal Hydrodnamic Models of Flat Micro Heat Pipes for Cooling of Multiple Electronic Components," *International Journal of Heat and Mass Transfer*, vol. 49, 2006, pp. 1375-1383.

[115] Y. Koito, H. Imura, M. Mochizuki, Y. Saito, & S. Torii, "Numerical Analysis and Experimental Verification on Thermal Fluid Phenomena in a Vapor Chamber," *Applied Thermal Engineering*, vol. 26, 2006, pp. 1669-1676.

[116] M.S. El-Genk, H.H. Saber, and J.L. Parker, "Efficient Spreaders for Cooling High-Power Computer Chips," *Applied Thermal Engineering*, vol. 27, 2007, pp. 1072-1088.

[117] R. Sonan, S. Harmand, J. Pelle, D. Leger, and M. Fakes, "Transient Thermal and hydrodynamic Model of Flat Heat Pipe for the Cooling of Electronics Components," *International Journal of Heat and Mass transfer*, vol. 51, no. 25-26, 2008, pp. 6006-6017.

[118] B. Xiao, & A. Faghri, "A Three-Dimensional Thermal-Fluid Analysis of Flat Heat Pipes," *International Journal Heat and Mass Transfer*, Vol.51, 2008, pp. 3113-3126.

[119] R. Ranjan, J.Y. Murthy, S.V. Garimella, and U. Vadakkan, "A Numerical Model for Transport in Flat Heat Pipes Considering Wick Microstructure Effects," *International Journal of Heat and Mass Transfer*, vol. 54, 2011, pp. 153-168.

Mohamed Chaker Zaghdoudi was born on September 4th, 1967 in Tunis (Tunisia). He received his engineer degree in Thermal Engineering from the National School of Engineering of Monastir (Tunisia) in 1992. Then, he received his M.Sc and PHD degrees in Thermal Engineering from the Institute of Applied Sciences of Lyon (France) in 1992 and 1996, respectively. In 2004, he received the ability degree to direct researches from the Institute of Applied Sciences of Lyon (France). Currently, he is Associate Professor at the Institute of Applied Sciences and Technology (Tunisia). Previously, he took up thermal R&D engineer posts within several industrial companies, and he was involved in many R&D European-funded projects. His R&D activities include the development and application of two-phase cooling systems and enhancement of heat and mass transfer in macro and micro scales. He has authored and co-authored many refereed articles most concentrating on two-phase heat transfer modeling and experimentation.

Samah Maalej was born on February 11th, 1972 in Makthar (Tunisia). She received his engineer degree in Thermal Engineering from the National School of Engineering of Monastir (Tunisia) in 1996. Then, she received his M.Sc and PHD degrees in Thermal Engineering from the Institute of Applied Sciences of Lyon (France) in 1997 and 2001, respectively. Since 2002, she has been an Assistant Professor at the Institute of Applied Sciences and Technology (Tunisia). Her R&D activities include the development and application of two-phase with or without phase change. She has authored and co-authored many refereed articles most concentrating on two-phase heat transfer modeling and experimentation.

Jed Mansouri was born on April 21st, 1979 in El-Kef (Tunisia). He received his engineer degree in Electro-Mechanical Engineering from the National School of Engineering of Sfax (Tunisia) in 2002. Then, he received his M.Sc degree in mechanical and manufacturing from the National School of

Engineering of Tunis (Tunisia) in 2004. Since 2005, he has been an Assistant (half-time) at the Institute of Applied Sciences and Technology (Tunisia). He is currently a Ph.D. candidate, and his research activities concern the cooling of dissipative electronic components using flat two-phase heat spreaders.

Mohamed Ben Hassine Sassi was born on October 31st, 1967 in Monastir (Tunisia). He received his engineer degree in Thermal Engineering from the National School of Engineering of Monastir (Tunisia) in 1993. Then, he received his M.Sc and PHD degrees in Thermal Engineering from the Institute of Applied Sciences of Lyon (France) in 1993 and 1997, respectively. He is an Assistant Professor at the Institute of Applied Sciences and Technology (Tunisia). His R&D activities include the development and application of solid-liquid phase change, inverse methods and their applications for thermal problems, and parameters and functions estimation. He has authored and co-authored many refereed articles.